In-depth exploration of the high and normal pH beef proteome: First insights emphasizing the dynamic protein changes in longissimus thoracis muscle from pasture-finished Nellore bulls over different postmortem times

Iliani Patinho, Daniel Antonelo, Eduardo Delgado, Laura Alessandroni, Julio C.C. Balieiro, Carmen Contreras-Castillo, Mohammed Gagaoua

In-depth exploration of the high and normal pH beef proteome: First insights emphasizing the dynamic protein changes in *Longissimus thoracis* muscle from pasture-finished Nellore bulls over different *postmortem* times

Iliani Patinho [1], Daniel S. Antonelo [2], Eduardo F. Delgado [3], Laura Alessandroni [4], Julio C.C. Balieiro [2], Carmen J. Contreras-Castillo [1] and Mohammed Gagaoua [5]*

[1] Department of Agri-food Industry, Food and Nutrition, Luiz de Queiroz College of Agriculture, University of Sao Paulo, Piracicaba, SP 13418-900, Brazil

[2] School of Veterinary Medicine and Animal Science, University of Sao Paulo, Pirassununga, SP 13635-900, Brazil

[3] Department of Animal Science, Luiz de Queiroz College of Agriculture, University of Sao Paulo, Piracicaba, SP 13418-900, Brazil

[4] Chemistry Interdisciplinary Project (CHIP), School of Pharmacy, University of Camerino, Via Madonna delle Carceri, 62032 Camerino, Italy

[5] PEGASE, INRAE, Institut Agro, 35590 Saint-Gilles, France

* Corresponding author e-mail: mohammed.gagaoua@inrae.fr

Abstract

This study aimed to evaluate for the first time the temporal dynamic changes in early *postmortem* proteome of normal and high ultimate pH (pHu) beef samples from the same cattle using a shotgun proteomics approach. Ten selected carcasses classified as normal (pHu < 5.8; n = 5) or high (pHu ≥ 6.2; n = 5) pHu beef from pasture-finished Nellore (*Bos indicus*) bulls were sampled from *Longissimus thoracis* muscle at 30 min, 9 h and 44 h *postmortem* for proteome comparison. The temporal proteomics profiling quantified 863 proteins, from which 251 were differentially abundant (DAPs) between high and normal pHu at 30 min (n = 33), 9h (n = 181) and 44h (n = 37). Among the myriad interconnected pathways regulating pH decline during *postmortem* metabolism, this study revealed the pivotal role of energy metabolism, cellular response to stress, oxidoreductase activity and muscle system process pathways throughout the early *postmortem*. Twenty-three proteins overlap among *postmortem* times and may be suggested as candidate biomarkers to the dark-cutting condition development. The study further evidenced for the first time the central role of ribosomal proteins and histones in the first minutes after animal bleeding. Moreover, this study revealed the disparity in the mechanisms underpinning the development of dark-cutting beef condition among *postmortem* times, emphasizing multiple dynamic changes in the muscle proteome. Therefore, this study revealed important insights regarding the temporal dynamic changes that occur in early *postmortem* of high and normal muscle pHu beef, proposing specific pathways to determine the biological mechanisms behind dark-cutting determination.

Keywords: Beef quality defects; Dark-cutting; Beef proteome; Energy metabolism; Nellore cattle; Oxidative stress; Bioinformatics; Biomarkers.

1. Introduction

Brazil has the largest bovine herd in the world and is the largest beef exporter, with a beef livestock agribusiness movement of approximately US$ 169.29 billion. Most of the Brazilian herd has influence of zebu cattle (*Bos taurus indicus*), mainly Nellore breed, which combine productivity, disease resistance and heat tolerance once animals are predominantly finished on pasture (ABIEC, 2022; Carvalho et al., 2014), but keeping in mind that a substantial amount of the animals are also reared under feedlot production systems (Ferraz & de Felício, 2010; de Andrade et al., 2020). However, although beef cattle have adapted well to tropical conditions in Brazil (Carvalho et al., 2014; Rodrigues et al., 2017; Malheiros et al., 2020), beef cattle finished in extensive systems (pasture-based) is usually darker in color appearance and produces a less tender cooked product than those finished in feedlot systems (grain-based) (Antonelo et al., 2022; Gómez et al., 2022) which may be directly related to the rate and extent of muscle pH decline. In fact, ultimate pH (pHu) is associated with muscle glycogen and *postmortem* energy metabolism. Several factors influence muscle pHu, including increased physical activity, feed deprivation, season, and pre-slaughter stress. These events are well-known to rapidly reduce muscle glycogen stores (Zhao et al., 2022; Terlouw et al., 2021; García-Torres et al., 2021) which leads to a high pHu (Poleti et al., 2018; Kiyimba et al., 2021) that negatively affect the final beef quality (Wu et al., 2020; England et al., 2016; Franco et al., 2015). As a result, carcasses with darker lean are generally downgraded during the process of grading, leading to significant economic losses globally for the beef sector (Gagaoua, Warner, et al., 2021; Ponnampalam et al., 2017). Thus, it is essential to avoid failures in the categorization of carcasses according to the pHu and develop early *postmortem* tools for their monitoring.

Several recent comprehensive reviews reported that proteomics techniques together with mass spectrometry (MS) and bioinformatics approaches have been widely used to show the mechanisms that drive the beef quality development in *postmortem* muscle, in addition to investigating the dynamic changes and modifications that occur in the muscle proteome and search for candidate biomarkers (Picard & Gagaoua, 2020; Gagaoua et al., 2021). Proteomics was successfully applied to the discovery of biomarkers of dark-cutting beef from *Bos taurus* (Franco et al., 2015; Mahmood et al., 2018; Poleti et al., 2018; Fuente-Garcia et al., 2019; Wu et al., 2020; Fuente-Garcia et al., 2020; Sentandreu et al., 2021; Kiyimba et al., 2022; 2023), however a

strong disparity (very weak overlap) among the studies was revealed using a meta-analysis integromics approach (Gagaoua et al., 2021). Although certain consistent pathways were reported, the authors evidenced a very weak overlap in the putative biomarkers among the eight dark-cutting beef proteomics studies (< 8%) with only 10 common protein biomarkers reported across no more than two studies. From the ten common proteins, eight were related to dark-cutting beef conditions in different directions (positive and negative). It was suggested that the molecular signatures underpinning dark-cutting beef development are more complex than expected, and exploratory studies of the muscle proteomes of the same animals at both early *postmortem* and at the usual sampling times used to categorized carcasses based on their high pHu (24 or 48h) would allow further insights on the biochemical mechanisms and discovery of more appropriate biomarkers.

Foreseeing the above, the current study used a shotgun proteomics approach to fill the gap in the early *postmortem* muscle metabolism, while considering *Bos indicus* cattle. We aim to evaluate using for the first time a serial-time analysis approaches the temporal dynamic changes in the abundances of the proteins that occur in high and normal muscle pHu carcasses sampled at three different times these being 30 min, 9 h and 44 h *postmortem*. The study further aimed to reveal new features behind the protein changes by considering new early *postmortem* sampling times along of the possibility of proposing a more robust list of biomarkers of dark-cutting beef condition.

2. Materials and Methods

All procedures used in this study were conducted in accordance with the Institutional Animal Care and Use Committee Guidelines (protocol 2019/22) and were approved by the committees of the “Luiz de Queiroz” College of Agriculture of the University of Sao Paulo.

2.1. Animals, treatments, and sampling

Ten carcasses classified as normal pHu beef (at 24, 48 and 72h *postmortem*) from pasture-finished Nellore (*Bos indicus*) bulls, ranging from 30 to 42 months of age (4 to 6 permanent incisors teeth) and 349 ± 31 kg of hot carcass weight were selected under industrial conditions. The carcasses were from a larger experiment at a commercial meat processor under standard slaughtering conditions (for further details refer to Patinho *et al.* (2024)). More specifically,

hundred carcasses were sampled from early *postmortem* time until 72h *postmortem*. The carcasses that were corresponding to the objectives of this study these being carcasses with normal pHu < 5.8; n = 5 or high pHu ≥ 6.2; n = 5 were targeted for the proteomics trial. For all the sampling times, samples (~ 30 g) were excised from the left side of the carcasses by targeting the *Longissimus thoracis* (LT) muscle adjacent between the 10^{th} and 11^{th} ribs immediately after skinning (approximately 30 min *postmortem*). The same carcasses, stored at 2 ± 2°C were further sampled from the same location at 9 h and 44 h *postmortem* following the same sampling conditions. All samples were immediately snap frozen in liquid nitrogen and stored at -80 °C for proteomics analyses.

2.2. pH determination and other meat quality evaluation

Muscle pH was determined using the iodoacetate method as described by Bendall (1978). Briefly, the three targeted sampling times for the proteomics analyses these being 30 min, 9 h and 44 h LT muscle samples, as well as the samples taken at 3 h, 6 h, 24 h and 72 h (all given in the pH decline curves of **Fig. 1**) were powdered, added to a buffer containing fresh 5 mM sodium iodoacetate and 150 mM KCl (pH 7.0) at a 1:8 ratio (wt/vol), and homogenized. Muscle homogenates were centrifuged at 13,000 ×g for 5 min at room temperature, equilibrated to 25 °C and measured using a digital pH meter (Lucadema, LUCA-210 model, São José do Rio Preto, Brazil) coupled with automatic temperature compensation and glass penetration electrode.

To ensure that the samples were correctly categorized as high pH (true dark-cutters) from normal pH, meat quality traits including color parameters: lightness (L^*), redness (a^*), yellowness (b^*), and computed chroma (C^*) and hue angle ($h°$), as well % Methmyoglobin (MetMb, %), % Deoxymyoglobin (DeoxyMb, %), % Oxymyoglobin (OxyMb, %) and Surface color stability), and texture traits: Warner-Bratzler shear force and drip loss%, were evaluated at 72h (**Table 1**) and details on the protocols are described in detail in previous studies (Gagaoua, Monteils, & Picard, 2018a; Patinho *et al.* (2024).

2.3. Proteome Analysis

2.3.1. Extraction and quantification of whole-muscle proteome

The frozen 30 min, 9 h and 44 h LT muscle samples from normal (n = 5) and high (n = 5) pHu sampled were powdered in liquid nitrogen. Then, 50 mg of ground tissue was homogenized in 0.5 mL of ice-cold lysis buffer containing 7 M urea, 2 M thiourea, 2% CHAPS, 1% dithiothreitol [DTT] and 1% phenylmethylsulfonyl fluoride [PMSF] for 45 s using a homogenizer (IKA, T10 model, Campinas, Brazil) (Bouley, Chambon, & Picard, 2004). Homogenates were then centrifuged at 12,000 × g for 30 min at 4 °C to remove debris (Zhu et al., 2021). The supernatants, which correspond to the total proteins, were collected and quantified using the Bradford Assay (#B6916, Sigma-Aldrich, St. Louis, USA) with bovine serum albumin (BSA) as the standard (Bradford, 1976).

2.3.2. Shotgun proteomics: LC-MS/MS analysis and protein quantification

For the preparation of the protein bands for shotgun proteomics analysis, the protein extracts stored at -80°C were first diluted with Milli-Q water following an in-house Excel spreadsheet calculator, adjusted to a final volume of 40 µg in an equal volume with fresh Laemmli denaturing buffer containing 125 mM Tris (pH 6.8), 4% w/v SDS, 10% v/v β-mercaptoethanol, 20% v/v glycerol, and 0.004% bromophenol blue (#S3401, Sigma-Aldrich, St. Louis, USA) and heated at 90 °C for 10 minutes (Lamri, della Malva, Djenane, Albenzio, & Gagaoua, 2023). The denatured protein extracts were then loaded in 10 wells (one gel for sampling each time) freshly prepared 12% resolving and 4% stacking gels in one-dimensional gel electrophoresis (1D sodium dodecyl sulfate polyacrylamide gel electrophoresis: SDS-PAGE) using a Mini-PROTEAN® Tetra Cell System (Bio-Rad, Hercules, CA, USA). The running of the electrophoresis, all the samples and gels together to avoid technical variability, was conducted using a TGS buffer containing 25 mM Tris (pH 8.6), 192 mM glycine and 0.1% SDS (#T7777, Sigma-Aldrich, Saint Louis, USA). The running conditions were set for 15 minutes at 4 watts to concentrate the proteins in one large band in the stacking gel.

The gels were carefully removed under sterile conditions, washed with fresh Milli-Q water, stained with EZ Blue Gel staining reagent (Sigma- Aldrich, Saint Louis, USA) for 15 min to clearly visualize the protein bands. The colored gels were then washed several times with Milli-Q water under gentle shaking. The protein bands carefully excised using sterile and disposable scalpels, immediately placed into sterile Eppendorf tubes to be reduced, alkylated, destained and dried, before liquid chromatography-tandem mass spectrometry (LC-MS/MS) analyses as

previously described (Lamri, della Malva, Djenane, López-Pedrouso, et al., 2023). For LC-MS/MS analysis, identification of the proteins and quantification, the dry protein bands were first digested by a sequence grade Trypsin (Promega, USA) following the steps described by (Lamri, della Malva, Djenane, Albenzio, & Gagaoua, 2023). The database search results were screened and exported when the false discovery rate (FDR) of the number of peptides is higher than 2 and the protein match level was <1%. The raw data from the LC-MS/MS were aligned against the *Bos taurus* database (https://www.uniprot.org/proteomes/UP000009136)

2.4. Statistical analyses

For the meat quality traits, a variance analysis (ANOVA) at a level of 5% (Tukey comparison) was performed to compare the pH values over *postmortem* time as well as for the comparison of the meat quality traits (pH, color and texture) evaluated at 72h *postmortem*. The whole meat quality data (pH, color and texture traits) were further projected in a principle component analyses (PCA) to highlight the degree of the relationships among the variables and their ability to separate the two pH groups (individuals) within the corresponding bi-plot. To check the suitability of the factorial model, the Kaiser-Meyer-Olkin (KMO) test for sampling adequacy was used and the overall KMO value is reported.

For the proteome data identified and quantified in the biological replicates of each pHu group and within each sampling time were considered in a pairwise manner for the statistical analyses. The database was uploaded to the online webservice MetaboAnalyst 5.0 tool (https://www.metaboanalyst.ca/) for analyses. First, the data were auto scaled prior to analysis and missing values (<3.1% of the database) were computed using the k-nearest neighbor algorithm. Second, the data were normalized by log-transformation and pareto scaling. For each sampling time, pairwise comparisons between the high *vs.* normal pHu were performed to analyze the protein abundances. Therefore, volcano plots were plotted and proteins with a minimum fold change of 1.2 and P-value < 0.05 were considered as regulated differently in the three comparison groups (high *vs.* normal pHu at 30 min, 9 h, and 44 h *postmortem*). The statistical comparisons were performed with adjusted P-values to Bonferroni correction.

2.5. Bioinformatics analyses

The gene names of the differentially abundant proteins (DAPs) were converted into human identifiers (gene names) based on the orthologous and homologous links, to avoid any limitation of the Gene Ontology (GO) annotations on bovine proteins as previously described (Gagaoua, Hughes, et al., 2020). For the GO analyses, the protein lists were analyzed using Metascape® webservice tool (https://metascape.org/) to identify the enriched pathways, clustering analyses of the GO terms and comparative heatmaps (hierarchical clustering of pathways) and network analysis. The parameters were set to proteins overlap > 3, an enrichment *P*-value < 0.05, and an enrichment factor > 1.5. Benjamini−Hochberg P-value correction algorithm and hypergeometric test were used to display the first statistically significant enriched ontology terms in each cluster. This approach provided a comprehensive gene list annotation curated via GO Biological Processes, GO Molecular Functions, Kyoto Encyclopedia of Genes and Genomes (KEGG) pathways and Reactome gene sets. For the protein-protein interactions (PPI), the STRING database (https://string-db.org/) was used to evaluate the known and predicted PPI among the different proteins lists for each of the three-*postmortem* time-points and within the common DAPs proteins. A confidence score of 0.500 was chosen as the minimum required interaction cutoff score with no additional interactors. The collected nodes of the subnetworks were used to create clusters of the corresponding DAPs (up-and down-regulated in the whole LT muscle proteome from high and normal pHu beef) using the Markov Clustering Algorithm (MCL) with an inflation parameter of 1.8. For the secretome analysis, the computational prediction of the putatively secreted proteins in bovine muscle through classical (involving a signal peptide) or non-classical way (without signal peptide on the sequence) was performed using the webservice open source ProteINSIDE tool (https://www.proteinside.org/).

3. Results

Unless for 30 min *postmortem* time, the pH declines curves were significantly different across all the sampling times considered (3 h, 6 h, 9 h, 24 h, 44 h and 72 h) between the normal and high pH carcasses evaluated in this trial (**Fig. 1A,B**). The variance analysis performed on the meat quality traits (**Table 1**) confirmed, differences in the pHu whatever the time of measurement (24 h, 44 h and 72h *postmortem*), lower lightness (*L**), redness (*a**), yellowness (*b**) and chroma (C*) values in high pH group, along of higher DeoxyMb, % and lower OxyMb, %. These results are in line to several studies in the literature including a recent similar study on *Bos taurus*

reported by Kiyimba *et al.* (2023). Tenderness evaluated by Warner-Bratzler shear force was also and as known in the literature lower in high pH group (36.85 N*)* compared normal pH group (96.08 N), evaluated in this trial at 72h *postmortem*. These results were further confirmed by the PCA given in **Fig. 2A** and the separation of the observations of the two pH groups in its bi-plot (**Fig. 2B**).

The shotgun proteomics allowed quantifying at an FDR of 1% and with a minimum of 2 peptides 863 proteins in the whole muscle samples (n = 5 normal pHu and n = 5 high pHu beef). The statistical comparison of the protein profiles in the proteome of LT muscle from normal and high pHu beef revealed 251 DAPs across the three *postmortem* times (30 min, 9 h and 44 h). Specifically, Volcano plot analyses allowed identifying 33, 181 and 37 DAPs for the proteome comparisons from normal and high pHu beef at 30 min (**Table 2**), 9 h (**Table 3**) and 44 h (**Table 4**) *postmortem*, respectively.

3.1. Comparison of the LT muscle proteome from normal and high pHu beef at 30 min *postmortem*

From the 33 DAPs identified in the LT muscle proteome to differ between normal and high pHu beef at 30 min *postmortem* (**Table 2**), 9 were up-regulated and 24 were down-regulated in high pHu beef (**Fig. 3A**). The pathway enrichment analysis of this protein list revealed 12 significant enriched terms (**Fig. 3B**). The top 5 enriched terms were “cellular response to stress”, “generation of precursor metabolites and energy”, “parkinson disease”, “nucleobase-containing small molecule metabolic process”, and “diseases of programmed cell death” (**Fig. 3C)**. The PPI network of the 33 DAPs is given in **Fig. 3D**. The network revealed interconnectedness among the functional pathways, mainly among four major pathways, these being TCA cycle and respiratory electron transport, calcium regulation, ribosome and proteasomes. The hierarchical heatmap clustering of the 33 up- and down-regulated proteins between high and normal pHu beef at 30 min *postmortem* revealed no common changing pathways. However, two terms related to cellular response to stress (R-HSA-2262752) and regulation of translation (GO:0006417) were exclusively enriched in high pHu beef only, while six terms related to parkinson disease (hsa05012), nucleobase-containing small molecule metabolic process (GO:0055086), generation of precursor metabolites and energy (GO:0006091), regulation of endocytosis (GO:0030100), carbohydrate metabolic process (GO:0005975), and calcium ion binding (GO:0005509) were

exclusively enriched in normal pHu beef only (**Fig. 3E**). The statistics details of each enriched term are given in **Table S1**.

3.2. Comparison of the LT muscle proteome from normal and high pHu beef at 9 h *postmortem*

As shown in **Table 3**, a higher number of proteins than 30 min *postmortem* (n = 181 DAPs) were identified to differ between normal and high pHu beef at 9 h *postmortem*. The results of the Volcano plot evidenced 77 up-regulated and 104 down-regulated in high pHu beef (**Fig. 4A**). The pathway enrichment analysis revealed 20 significantly enriched terms (**Fig. 4B**). Among these, the top 5 enriched ones were related in the following order to "generation of precursor metabolites and energy", "cellular response to stress", "muscle structure development", "axon guidance" and "muscle system process" (**Fig. 4C**). The PPI network revealed a strong interconnectedness between the proteins and the functional pathways to which they belong (**Fig. 4D**). To the best of our knowledge, this is the first comprehensive PPI network depicting the dynamic changes occurring in early (9 h) *postmortem* muscle of dark-cutting beef as revealed by shotgun proteomics. Such complexity of the mechanisms is further confirmed by the hierarchical heatmap clustering of the up- and down-regulated proteins between high and normal pHu beef at 9 h *postmortem* (**Fig. 4E**). The findings revealed 14 common changing pathways, including generation of precursor metabolites and energy (GO:0006091), cellular response to stress (R-HAS-2262752), muscle system process (GO:0003012), and oxidoreductase activity (GO:0016491). Interestingly, one term was exclusively enriched in high pHu beef only, this being regulation of ryanodine-sensitive calcium-release channel activity (GO:0060314), while five terms were exclusively enriched in normal pHu beef only, including muscle cell development (GO:0055001) and structural constituent of muscle (GO:0008307). The statistics details of each enriched term are given in **Table S2**.

3.3. Comparison of the LT muscle proteome from normal and high pHu beef at 44 h *postmortem*

From the 37 DAPs identified in the LT muscle proteome to differ between normal and high pHu beef at 44 h *postmortem* (**Table 4**), 19 were up-regulated and 18 were down-regulated in high pHu beef (**Fig. 5A**). The pathway enrichment analysis revealed 19 significantly enriched

terms (**Fig. 5B**). Among these, the top 5 enriched terms were oxidoreductase activity, generation of precursor metabolites and energy, glutathione metabolic process, locomotory behavior and chaperone binding (**Fig. 5C**). The PPI network of the 37 DAPs revealed an interconnectedness among the proteins and the functional pathways to which they belong (**Fig. 5D**). The hierarchical heatmap clustering of the up- and down-regulated proteins between high and normal pHu beef at 44 h *postmortem* (**Fig. 5E**) revealed one common changing pathway related to oxidoreductase activity (GO:0016491). Five terms were exclusively enriched in high pHu beef only, including NAD binding (GO:0051287) and muscle system process (GO:0003012), while six terms were exclusively enriched in normal pHu beef only, including regulation of oxidative stress-induced intrinsic apoptotic signaling pathway (GO:1902175) and response to hypoxia (GO:0001666). The statistics details of each enriched term are given in **Table S3**.

3.4. Protein overlap and comparison of the DAPs changing during the *postmortem* period

Functional enrichment analysis and clustering on the total DAPs identified to change in the LT muscle proteome from normal and high pHu beef among the three *postmortem* time comparisons are given in **Fig. 6**. The overlap among the three protein lists revealed 23 common proteins: ALDH2, ANK1, ANXA4, ATP5B, CYB5R3, CYC1, DNAJA2, FHL1, GAPDH, GSTM2, IDH3B, IDH3G, MB, NDUFA7, NDUFA9, SERPINA3, SERPINC1, SLC25A3, SOD1, TMOD1, TUBA1B, UBE2L3 and UNC45B (**Fig. 6A**). These proteins belong to eight significantly enriched GO terms (**Fig. 6B**) mainly dominated by oxidoreductase activity (GO:0016491) and generation of precursor metabolite and energy (GO: 0006091) (**Fig. 6C**). The relative abundance of the 23 DAPs proteins are clustered in the heatmap (**Fig. 6D**) using the averages of pH group/pH to highlight the proteins mainly up in high pHu and those Down in high pHu. The PPI network of the 23 overlap proteins revealed a strong interconnectedness among the proteins and a domination of the TCA cycle and respiratory electron transport (**Fig. 6E**). The hierarchical heatmap clustering of the total DAPs of each *postmortem* time (30 min, 9 h and 44 h) revealed five common enriched terms (**Fig. 6F**), these being generation of precursor metabolite and energy (GO: 0006091), cellular response to stress (R-HAS-226752), chaperone binding (GO:0051087), oxidoreductase activity (GO:0016491) and muscle structure development (GO:0061061). All of these terms were more abundant at 9 h *postmortem*, except for the chaperone binding that was more abundant at 44 h *postmortem*. Moreover, it must be noted that

the cellular response to chemical stress (R-HSA-9711123), NADH metabolic pathway (GO:0006734), cardiac muscle contraction (hsa04260), platelet degranulation (R-HSA-114608), structural constituent of muscle (GO:0008307), alpha-actinin binding (GO:0051393) and actin binding (GO:0003779) were significantly and exclusively specific to the LT muscle proteome at 9 h *postmortem*. The secretome analyses (**Fig. 7**) further evidenced more proteins (n = 12) that are secreted either through the classical (n = 8) or the non-classical pathways (n = 4) at 9h *postmortem* compared to the protein lists of the 30min (n = 2) and 44h *postmortem* (n = 1). The only protein secreted through the classical pathway (extracellular protein) was SERPINC1, which was common with the 9h *postmortem* (**Fig. 7**). This protein also known as antithrombin-III belongs to the superfamily of serpins, previously reviewed for their major role in meat tenderization (Gagaoua, Hafid, et al., 2015).

3.5. Comparison of DAPs proteins of this study with Gagaoua's dark-cutting beef proteome database

The input proteins identified in this trial were matched against the dark-cutting beef proteome database previously built in the integromics study by Gagaoua, Warner, et al. (2021). The results revealed 28 common proteins whatever the *postmortem* time (**Fig. 8**). More specifically, at 30 min *postmortem*, ATIC, MDH1 and UGP2 were the common proteins (**Fig. 8A**). The hierarchical heatmap clustering of the DAPs revealed 8 common enriched GO terms (**Fig. 8D**). Interestingly, 12 enriched terms were significantly and exclusively specific to Gagaoua's database. At 9 h *postmortem*, 23 (ACTA1, ACTN2, ATP5B, BLMH, CACNB1, CKM, CMYA5, COPS7A, COQ8A, COX6A2, EPM2A, FHL1, LDB3, LMCD1, MYOM2, MYOT, NME2, PDLIM5, PGAM2, PHKB, PKM2, PRKAA2, UQCRC2) proteins overlapped between datasets (**Fig. 8B**). The hierarchical heatmap clustering of the DAPs revealed 16 common enriched terms (**Fig. 8E**), from which only 3 cluster terms were exclusively enriched in the Gagaoua's database, these being actin-myosin filament sliding (GO:0033275), glycogen metabolism (R-HAS-8982491) and protein homodimerization activity (GO:0042803), while one term was exclusively enriched in the present work, this being oxidoreductase activity, acting on the aldehyde or oxo group of donors, NAD or NADP as acceptor (GO:0016620). At 44 h *postmortem*, two proteins (DHRS7B and FHL1) overlapped between studies (**Fig. 8C**). The hierarchical heatmap clustering of the DAPs revealed seven common enriched terms (**Fig. 8F**). Interestingly, one term was exclusively

enriched in the present database, this being NAD binding (GO:0051287), while 12 terms were exclusively enriched in the Gagaoua's database only.

4. Discussion

The global beef chain has been directed to meet the beef quality demands of the market and consumers expectations. Purchasing decisions are primarily driven by lean beef color as consumers often consider color an indicator of freshness and wholesomeness (Suman & Joseph, 2013). For this reason, dark-cutting carcasses are discounted during meat grading and downgraded in value, leading to economic losses for the beef sector (Ponnampalam et al., 2017). The dark-cutting condition usually arises after cattle experience physical and psychological stress caused by several negative *ante mortem* factors such that muscle glycogen is depleted, hence impacting the rate of pH decline resulting in abnormally dark muscles (Terlouw et al., 2021; Ponnampalam et al., 2017; Tarrant, 1989). Thus, there is a need to strengthen our knowledge on the factors underpinning the biochemical mechanisms at interplay in meat quality traits development including dark-cutting beef condition.

The application of proteomics in meat research has recently yielded valuable insights on the biochemical processes underpinning meat quality development and variability over conventional biochemistry methods (Purslow, Gagaoua, & Warner, 2021; Gagaoua et al., 2024), hence contributing greatly to a better understanding of the complexity of the muscle proteome and its importance in determining several meat quality traits (Gagaoua, Schilling, Zhang, & Suman, 2022). Several recent studies reviewed in the Gagaoua's integromics meta-analysis (Gagaoua, Warner, et al., 2021) have used multiple approaches likely label-free proteomics, two-dimensional gel electrophoresis or OFFGEL proteomics approaches (Franco et al., 2015; Fuente-Garcia et al., 2019; Fuente-Garcia et al., 2020; Hughes, Clarke, Li, Purslow, & Warner, 2019; Kiyimba et al., 2021; Mahmood, Turchinsky, Paradis, Dixon, & Bruce, 2018; Poleti et al., 2018; Wu et al., 2020; Sentandreu et al., 2021) to decipher the mechanisms related to the dark-cutting development. All these studies focused on muscle samples taken 24 h or 48 h *postmortem*, which correspond also to the same time of pHu measurement on the chilled carcasses. However, to date and to the best of our knowledge, shotgun proteomics approach coupled with in-depth bioinformatics and applied in a serial time analysis to investigate the dynamic changes in early *postmortem* proteome of dark-cutting beef have never been studied.

In this study, the temporal proteomics (analyses of the muscle proteomes at several *postmortem* times of the same carcasses) of the LT *postmortem* muscle from normal and high pHu beef evidenced substantial dynamic changes along with the involvement of myriad and interconnected biological pathways, some of which were never revealed before to be related with dark-cutting beef determination. Interestingly, the hierarchical heatmap (**Fig. 6**) revealed that the significant enrichment of "generation of precursor metabolites and energy", "cellular responses to stress", "chaperone binding", "oxidoreductase activity" and "muscle structure development" are common features and demonstrated to be the central role in driving the dark-cutting beef development. In addition, insights on how these complex and interconnected pathways are changing as the dark-cutting beef develops at each *postmortem* time are for the first time revealed. In the following sections, we discuss in-depth the functions and metabolic pathways to which certain of the DAPs belong, some of which may be proposed as candidate biomarkers to monitor the dynamic changes in early *postmortem* (30 min, 9 h and 44 h) proteome of dark-cutting beef.

4.1. Pivotal role of energy metabolism at 30 min *postmortem*

As expected, the energy metabolism was identified as one of the major signatures characterizing the differences in the LT muscle proteome between normal and high pHu beef at 30 min *postmortem* (**Fig. 3**). Interestingly, all the DAPs belonging to the TCA cycle (UGP2, ATIC and MDH1), mitochondrial respiration (ATP5B and NDUFA9) and β-oxidation (HADHA and ADIPOQ), which are known mechanisms responsible for producing energy during the initial events of the *postmortem* metabolism, were down-regulated in dark-cutting beef compared to normal-pH beef. UGP2, an enzyme involved in glycogen biosynthesis (Pescador et al., 2010), was up-regulated in normal-pH beef, suggesting lower glycogen or weak breakdown during peri-slaughter events in dark-cutting beef. Poleti et al. (2018) reported a greater abundance of UGP2 in muscle with higher glycogen concentration, which produced a normal-pH at 24 h *postmortem*. ATIC was also down-regulated in dark-cutting beef, which may have decreased the IMP/AMP (Antonelo et al., 2022) levels resulting in a lower phosphofructokinase activation and consequently decreased glycolysis (England, Matarneh, Scheffler, Wachet, & Gerrard, 2015), as also observed in earlier studies (Shen, Gerrard, & Du, 2008). Thus, as long as the glycolytic enzymes are not inhibited by the low pH during the early *postmortem* metabolism, glycolysis will

continue to contribute to the pH decline, as observed by the negative correlation of $pH_{45\ min}$ with MDH1 (Gagaoua, Terlouw, et al., 2015), a protein that plays an essential role in the TCA cycle, further involved in apoptosis onset (Lee, Kim, Cho, & Youn, 2009).

Furthermore, *postmortem* energy metabolism and the rate of pH decline can also be affected by mitochondria (Dang et al., 2020; Matarneh, Yen, Bodmer, El-kadi, & Gerrard, 2021). The mitochondrial β-oxidation pathway is the major energy-producing process in tissues and is performed through consecutive reactions with a breakdown of fatty acids into acetyl-CoA. It has been reported that lipids, the essential regulators of cellular stabilization and metabolism, have a pivotal role in *postmortem* energy production and in sustaining the needed energy during early *postmortem* for cell death processes such as apoptosis (Ouali et al., 2013).

Interestingly, in the present study, HADHA and ADIPOQ were up-regulated in normal-pH beef, which suggests a more intense mitochondrial β-oxidation. Matarneh et al. (2017) showed that intact mitochondria slowed the rate of pH decline during the first 30 min *postmortem*, stabilizing ATP levels and reducing glycolytic flux. However, after 2 h *postmortem*, mitochondria have increased ATP hydrolysis, glycogen breakdown, lactate accumulation, and pH decline, which was associated to the activation of the ATP5B, named ATP synthase (F_1F_0 ATP synthase or Complex V), an important protein in the production of ATP from ADP in the respiratory chain (Matarneh, Beline, Luz, Shi, & Gerrard, 2018). Accordingly, another earlier study by Ishii, Shirai, Makino, & Nishikata, (2014) demonstrated that ATP5B increases ATP hydrolysis and then glycolytic flux. A very recent study by Schulte et al. (2022) reported a lower pH 1 h *postmortem* associated with a more intense glycolysis in normal-pH beef when compared to dark-cutting beef.

In the present study and for Nellore cattle, the lower abundance of mediators of the β-oxidation, TCA cycle and mitochondrial electron transport chain, which may suggest a lower mitochondrial activity even under energy deprivation, significantly contribute to delaying the rate and extent of pH decline during early *postmortem* in high pHu beef, which partially explain the initial events of the dark-cutting development, since this effect may be cumulative over *postmortem* time (Matarneh et al., 2018).

4.2. Pivotal role of ribosomal proteins and histones on the cellular response to stress at 30 min *postmortem*

The cellular responses to stress was identified as the major signature characterizing the differences in the LT muscle proteome between normal and high pHu beef at 30 min *postmortem* (**Fig. 3**). Among the candidate biomarkers, ribosomal proteins (RPL18A, RPL24, RPS9 and RPS18) were the central proteins to modify this pathway in dark-cutting beef. Greater abundance of ribosomal proteins may suggest that several proteins experiencing changes during early *postmortem* metabolism, as a resilient response of muscle cells to energy deprivation (Ubaida-Mohien et al., 2019), would play essential roles for the energy-demanding cell-death processes such as autophagy and apoptosis (Ouali et al., 2013).

In this study, EIF5A, a p53/TP53-dependent regulator of apoptosis that can be activated temporarily to promote cell survival and permanently to stimulate cell death (Green, Galluzzi, & Kroemer, 2014), was also up-regulated in dark-cutting beef. Such apoptotic stimulation can be achieved through mitochondrial Ca^{2+} overload (Giorgi et al., 2015), which inhibits autophagy, thereby delaying apoptosis onset (Tasdemir et al., 2008) and consequently activating the pro-apoptotic factors such as Bcl-2. In this sense, greater abundance of calcium regulation proteins (CAM2KA and CALR) is in good agreement with the cell deaths roles (apoptosis and autophagy) of EIF5A in dark-cutting beef.

Furthermore, greater abundance of histones (HIST3H2BB and HIST1H2AJ) observed to impact on the cellular responses to stress pathway in dark-cutting beef may be associated to the hallmarks of apoptosis, such as DNA fragmentation, condensation of chromatin and actin degradation, detected in muscles during the *postmortem* storage period (Gagaoua et al., 2015; Longo, Lana, Bottero, & Zolla, 2015; Ouali et al., 2013). Therefore, this study reveals for the first time a pivotal role of ribosomal proteins and histones in Nellore *Bos indicus* cattle as a response to stress, hence confirming recent findings on *Bos taurus* cattle reported by Kiyimba et al. (2023). Further studies are warranted to decipher their roles on the initial events of the dark-cutting beef development.

4.3. Pivotal role of energy metabolism and cellular response to stress on muscle structure and development at 9 h *postmortem*

A strong interconnectedness between the proteins and the functional pathways to which they belong was depicted in early (9 h) *postmortem* muscle. The findings revealed 14 common changing pathways, including the aforementioned energy metabolism and cellular responses to stress. The identification of a high number of DAPs from the energy metabolism pathway early *postmortem* phase is in a good agreement with previous studies (Gagaoua, Warner, et al., 2021; Gagaoua, Terlouw, Richardson, Hocquette, & Picard, 2019; Fuente-Garcia et al., 2020). Among them, UQCR1 and UQCR2 were down-regulated in dark-cutting beef. These subunits of the cytochrome bc1 complex are part of the mitochondrial respiratory chain involved in electron transport during oxidative phosphorylation and ATP synthesis (Mato et al., 2019) and have been associated to a normal pHu decline and beef color stability (Suman, Wang, Gagaoua, Kiyimba, & Ramanathan, 2023; Poleti et al., 2018; Yu et al., 2017). Moreover, several mediators of glycolysis were up-regulated in normal-pH beef, such as PKM and ENO3. Earlier studies from Spain on young bulls by Fuente-Garcia et al. (2020) and Sierra et al. (2021) further reported lower PKM abundance in high pHu beef, which can be explained by the early glycogen depletion causing a decrease in the glycolytic flux, as suggested in this study by the up-regulation of UGP2 in dark-cutting beef at 30 min *postmortem*. The glycolytic enzyme ENO3 plays an important role in pH decline and *postmortem* metabolism (Gagaoua, Bonnet, Ellies-Oury, Koning, & Picard, 2018b) and its down-regulation indicates a cellular stress response to deprivation of oxygen supply and differences in glucose levels (Sedoris, Thomas, & Miller, 2010). Furthermore, it was possible to observe that ENO3 interacts with other proteins in the PPI network (**Fig. 4D**), for example, heat shock proteins (Wulff, Jokumsen, Højrup, & Jessen, 2012), contractile proteins (Hughes, Clarke, Li, Purslow, & Warner, 2019) and oxidative stress (Gagaoua, Terlouw, Boudjellal, & Picard, 2015), showing the complex interactions involved in the pHu determination process.

Interestingly, in the present study, two heat shock proteins, HSPA8 and HSPA5, were observed to be up- and down-regulated, respectively, in dark-cutting beef at 9 h *postmortem*. HSPA8, known as HSP70, is an inducible HSP that is involved in several underlying mechanisms of meat tenderization (Gagaoua, Terlouw, et al., 2021), such as in the transport of proteins into the mitochondria (Wiedemann, Frazier, & Pfanner, 2004), in muscle structure, by binding to structural proteins or regulate cell signaling pathways (Daugaard, Rohde, & Jäättelä, 2007; Zhu et al., 2021) and in oxidative stress, by sequestering pro-apoptotic factors (Jiang et al., 2011).

However, HSPA5 (HSP70 family) has chaperone activity due to its binding to Ca^{2+}, which corresponds to 25% of the Ca^{2+} reserves in the sarcoplasmic reticulum (Lièvremont, Rizzuto, Hendershot, & Meldolesi, 1997). Thus, when Ca^{2+} reserves decreasing or depleted, there is a greater amount of proteins in the sarcoplasmic reticulum leading to increased HSPA5 expression (Coe & Michalak, 2009). As HSPA5 is located mainly within the sarcoplasmic reticulum, the greater abundance of this HSP could be related to muscle fibers, since fast-twitch glycolytic fibers have a greater volume of sarcoplasmic reticulum (Rodrigues et al., 2017; Baylor & Hollingworth, 2012). Therefore, during *postmortem* time, apoptosis can affect skeletal muscle integrity through the modulation of Ca^{2+} flow with implications on muscle ultrastructural changes, hence playing a pivotal role in the determination of final meat quality (Gagaoua, Terlouw, et al., 2021; Gagaoua, Troy, & Mullen, 2021; Purslow, Gagaoua, & Warner, 2021).

In the present study and at 9h *postmortem*, muscle cell development and structural constituent of muscle were identified to be exclusively enriched in normal pHu beef only (**Fig. 4E**), which may indicate a severe disorganization of the sarcomere during early *postmortem* in normal-pHu beef due to a disruption of sarcoplasmic reticulum caused by apoptosis, hence increasing the activation of the endogenous proteases such as calpains and caspases, with central roles in proteolysis (Ertbjerg, 2022). Among the changing proteins, ACTA1, ACTN2, CAPN3 and MYOM2 participate in both enriched terms and were up-regulated in normal pHu compared to high pHu beef at 9 h *postmortem*. ACTA1 is the first protein targeted by caspases and is considered as a good hallmark of apoptosis onset (Ouali et al., 2013) while ACTN2 is an actin-binding protein that is the main component of skeletal muscle fibers, being expressed only in fast-twitch muscle fibers exhibiting high glycolytic activity (Lek, Quinlan, & North, 2009). The recent proteomics study by Schulte et al. (2022) demonstrated that similar abundances of HSP27 and ACTA1 may indicate an earlier onset of both apoptosis and *rigor mortis* in normal-pHu when compared to high-pHu beef. Moreover, CAPN3, the major intracellular protease, is especially found in type II fibers (Ojima et al., 2010). The down-regulation of HSP70 and CAPN3 in normal pHu may influence beef color determination (Gagaoua, Terlouw, et al., 2015) by changing reflectance and light scattering at the surface of meat cuts (Gagaoua, Terlouw, & Picard, 2017; Purslow, Gagaoua, & Warner, 2021). MYOM2, a structural protein, is also expressed in glycolytic fibers and has recently been associated to CKM expression (Gagaoua, Troy, & Mullen, 2021) since the rate of CKM fragmentation influences the rate of energy

depletion and the pH decline. Thus, the proposed disorganization of sarcomere during early *postmortem* in normal-pHu beef due to the proteolytic activity is closely related to the more glycolytic muscle metabolism when compared to the oxidative muscle metabolism in dark-cutting beef.

4.4. Pivotal role of oxidoreductase activity and oxidative stress at 44 h *postmortem*

The oxidoreductase activity was identified as the major signature characterizing the differences in the LT muscle proteome between normal and high pHu beef at 44 h *postmortem* (**Fig. 5**). Among the DAPs observed to be constitutive of this pathway, NDUFA7 (Complex I), NDUFA9 (Complex I) and CYC1 (Complex III) were up-regulated in normal-pHu beef while IDH3G was up-regulated in dark-cutting beef. To date and to the best of our knowledge, CYC1 was identified for the first time in this study to be associated with dark-cutting beef. CYC1 is a component of ubiquinol-cytochrome c oxidoreductase, a transmembrane complex of several subunits that is part of the mitochondrial electron transport chain that drives oxidative phosphorylation (Shojapour, Fatemi, Farahmand, & Shasaltaneh, 2021). IDH3G catalyzes the oxidative decarboxylation of isocitrate to 2-oxoglutarate in the TCA cycle, allowing for the concomitant reduction of NAD+ to NADH, which is then used to generate ATP through the electron transport chain (Okamoto et al., 2003). NADH is required in the electron transport chain for maximum ATP production (Gagaoua, Terlouw, et al., 2015), which promotes mitochondrial respiration and metmyoglobin reduction (Tang et al., 2005), thereby influencing the stability of beef color (Suman, Wang, Gagaoua, Kiyimba, & Ramanathan, 2023). Greater abundance of TCA intermediates along with an increased mitochondrial respiration capacity may be a conducive factor for increased mitochondrial oxygen consumption, thus contributing to muscle discoloration via myoglobin deoxygenation, producing dark-cutting beef (Gagaoua, Warner, et al., 2021; Kiyimba et al., 2022; Suman et al., 2023).

Although normal-pHu beef showed a higher impact on oxidoreductase activity, which proposes greater muscle discoloration as confirmed in the results of **Table 1**, several proteins related to the regulation of oxidative stress were up-regulated in this group, such as CYB5R3, DHRS7B, SOD1, SOD2 and PARK7, therefore suggesting greater color stability. For example, CYB5R3 is involved in many oxidation and reduction reactions, such as the reduction of methemoglobin to hemoglobin (Elahian, Sepehrizadeh, Moghimi, & Abbas, 2014). The study by

Zhai, Djimsa, Prenni, Woerner, & Belk (2020) reported that a greater abundance of CYB5R3 increases metabolic stability, inhibits the pro-apoptotic activity of the protein, increases autophagy and, among other functions, promotes late apoptosis in the LT muscle during the *postmortem* period. Like CYB5R3, DHRS7B is an oxidoreductase dependent on NAD or NADP as an acceptor and can promote exogenous carbonyl metabolism (Stambergova, Skarydova, Dunford, & Wsol, 2014), in which its overexpression may be beneficial to reduce carbonyl toxicity to cells in normal-pHu beef (Wu et al., 2020). SOD1 and SOD2 are two of the three superoxide dismutases responsible for destroying free superoxide radicals, acting as an antioxidant factor. López-Pedrouso et al. (2022) also reported a greater abundance of SOD2 in normal-pHu foal followed by a higher color stability. Moreover, PARK7 plays an important role against oxidative stress and cell death and previously reported as a robust biomarker of beef color (Gagaoua, Hughes, et al., 2020). PARK7 can interact with other pathways, such as heat shock proteins (Wu et al., 2020) and energy metabolism proteins (Picard & Gagaoua, 2020), thus delaying apoptotic processes (Gagaoua, Terlouw, et al., 2021) and influencing the ultimate pH and meat tenderization processes. Previous studies have also reported that PARK7 plays a role in determining beef color via mitochondrial protection (Gagaoua, Terlouw, & Picard, 2017; Yang et al., 2018; Wu et al., 2015). Therefore, the high levels of reactive oxygen species, the lack of response to oxidative stress, as well as a weak protein folding response may be other relevant pathways that promote dark-cutting beef condition (Gagaoua, Warner, et al., 2021), which were all observed in the present study.

4.5. Comparison of the candidate dark-cutting beef protein biomarkers with the literature

To gain further mechanistic insights on the underpinning pathways related to dark-cutting beef development, functional annotations comparing the DAPs found in this study over *postmortem* time with the dark-cutting beef proteome database described in a previous integromics meta-analysis (Gagaoua, Warner, et al., 2021) were performed. The protein overlaps of the two proteome repertoires showed 3, 23 and 2 common proteins at 30 min (**Fig. 8A)**, 9 h (**Fig. 8B)** and 44 h (**Fig. 8C)** *postmortem*, respectively, mainly belonging to three biological pathways: energy metabolism proteins, muscle structural proteins and response to oxidative stress. These findings together with the previous conclusions from the integromics meta-analysis underline the importance of energy metabolism, oxidative stress and muscle system process on the dark-cutting

beef development (**Fig. 8D-F**). Interestingly, the protein FHL1 was up-regulated in high pHu beef at 9 and 44 h *postmortem* (**Fig. 8B-C**), which may be considered as a putative biomarker for dark-cutting condition. FHL1 is recognized as a multifunctional protein, among which it acts in cell proliferation, apoptosis and interacts with metabolic enzymes in response to oxidative stress in muscle (Shathasivam, Kislinger, & Gramolini, 2010). In addition, it can regulate calcium homeostasis (Pillar et al., 2017), having an important role in determining the beef pHu and tenderness (Gagaoua, Bonnet, & Picard, 2020) since Ca^{2+} ions can contribute to the regulation of energy metabolism pathways (Carafoli, 2002) and also affect the enzymatic speed of several metabolic enzymes (Picard & Gagaoua, 2017). The up-regulation of FHL1 was also associated to the weakening of the Z-line in high pHu beef, as it is involved in the assembly of the cellular cytoskeleton structure (Hughes, Clarke, Purslow, & Warner, 2019). In this sense, Lomiwes, Farouk, Wu, & Young (2014) reported that high pHu muscles showed greater degradation of cytoskeletal proteins, such as titin, nebulin and filamin, associated with a up-regulation of FHL1. The results further revealed a weak overlap in the common proteins, especially at 48h *postmortem*, the usual timing used to assess the proteome-basis of dark-cutting beef in previous study. The confirmed disparity in the protein overlap among dark-cutting beef proteomics study warrants special attention to consider the multidimensional factors behind this quality defect condition.

5. Conclusion

This study revealed important insights regarding the dynamic changes that occur in early *postmortem* of normal and high muscle pHu beef, validating specific biochemical pathways to determine the biological mechanisms underpinning the dark-cutting development. In comparison to the previous proteomics studies on dark-cutting beef that used 24 or 48 *postmortem* sampling times only, this study added novel knowledge on the complexity of the mechanisms when they were explored in a temporal manner by additionally considering sampling times of 30 min and 9h *postmortem*. Moreover, the temporal shotgun proteomics coupled with an in-depth bioinformatics analysis allowed for the first time to evidence the dynamic time-course changes and disparity in the molecular signatures underpinning the dark-cutting beef condition development. The pivotal role of energy metabolism, cellular response to stress, muscle system process and oxidoreductase activity were significantly revealed throughout the early *postmortem* metabolism in Nellore *Bos*

indicus cattle. Twenty-three proteins overlap among *postmortem* times (30 min, 9 h and 44 h *postmortem*) and may be suggested as candidate biomarkers to monitor the proteome changes in the dark-cutting development. Moreover, it is interesting to underline that ribosomal proteins and histones were revealed to affect significantly the cellular response to stress during the initial events of dark-cutting development. Finally, the sampling time seemed a key factor in exploring the underlying mechanisms of dark-cutting beef, hence asking for standardization of the time allowing the discovery of biomarkers of this quality defect to allow generic comparisons among studies. This would further reduce the large disparity we are still observing in the proteomics studies of dark-cutting beef condition.

CRediT authorship contribution statement

Iliani Patinho: Conceptualization, Data curation, Formal Analysis, Investigation, Methodology, Visualization, Writing – original draft. **Daniel S. Antonelo:** Formal Analysis, Software, Visualization, Writing – review & editing. **Eduardo F. Delgado:** Writing – review & editing. **Laura Alessandroni:** Data curation, Formal Analysis, Visualization, Writing – review & editing. **Julio C.C. Balieiro:** Supervision, Writing – review & editing. **Carmen J. Contreras-Castillo:** Conceptualization, Funding acquisition, Supervision, Writing – review & editing. **Mohammed Gagaoua:** Conceptualization, Data curation, Formal Analysis, Funding acquisition, Investigation, Methodology, Project administration, Resources, Software, Supervision, Validation, Visualization, Writing – original draft, Writing – review & editing

Acknowledgments

This work was supported by the São Paulo Research Foundation FAPESP (grant # 2017/26667-2; 2019/26026-2).

Conflict of interest

No potential conflict of interest was reported by the authors.

References

ABIEC. (2022). Beef Report–Perfil da Pecuária no Brasil. *Associação Brasileira das Indústrias Exportadoras de Carnes.* Retrieved from https://www.abiec.com.br/publicacoes/beef-report-2022/

Antonelo, D. S., Gómez, J. F. M., Silva, S. L., Beline, M., Zhang, X., Wang, Y., … Balieiro, J. C. C. (2022). Proteome basis for the biological variations in color and tenderness of longissimus thoracis muscle from beef cattle differing in growth rate and feeding regime. *Food Research International*, *153*, 110947. https://doi.org/10.1016/j.foodres.2022.110947

Antonelo, D. S., dos Santos-Donado, P. R., Ferreira, C. R., Colnago, L. A., Ocampos, F. M. M., Ribeiro, G. H., … Balieiro, J. C. C. (2022). Exploratory lipidome and metabolome profiling contributes to understanding differences in high and normal ultimate pH beef. *Meat Science*, *194*, 108978. https://doi.org/10.1016/j.meatsci.2022.108978

Baylor, S. M., & Hollingworth, S. (2012). Intracellular calcium movements during excitation-contraction coupling in mammalian slow-twitch and fast-twitch muscle fibers. *Journal of General Physiology*, *139*(4), 261–272. https://doi.org/10.1085/jgp.201210773

Bendall, J. R. (1978). Variability in rates of pH fall and of lactate production in the muscles on cooling beef carcasses. *Meat Science*, *2*(2), 91-104. https://doi.org/10.1016/0309-1740(78)90010-4

Bouley, J., Chambon, C., & Picard, B. (2004). Mapping of bovine skeletal muscle proteins using two-dimensional gel electrophoresis and mass spectrometry. *Proteomics*, *4*, 1811–1824. https://doi.org/10.1002/pmic.200300688

Bradford, M. M. (1976). A Rapid and Sensitive Method for the Quantitation of Microgram Quantities of Protein Utilizing the Principle of Protein-Dye Binding. *Analytical Biochemistry*, *72*(1–2), 248–254. https://doi.org/https://doi.org/10.1016/0003-2697(76)90527-3

Carafoli, E. (2002). Calcium signaling: A tale for all seasons. *PNAS*, *99*(3), 1115–1122. https://doi.org/10.1073/pnas.032427999

Carvalho, M. E., Gasparin, G., Poleti, M. D., Rosa, A. F., Balieiro, J. C. C., Labate, C. A., … Coutinho, L. L. (2014). Heat shock and structural proteins associated with meat tenderness in Nellore beef cattle, a Bos indicus breed. *Meat Science*, *96*(3), 1318–1324. https://doi.org/10.1016/j.meatsci.2013.11.014

Coe, H., & Michalak, M. (2009). Calcium binding chaperones of the endoplasmic reticulum. *Gen Physiol Biophys*, *28*, F96–F103.

Dang, D. S., Buhler, J. F., Davis, H. T., Thornton, K. J., Scheffler, T. L., & Matarneh, S. K. (2020). Inhibition of mitochondrial calcium uniporter enhances postmortem proteolysis and tenderness in beef cattle. *Meat Science*, *162*, 108039. https://doi.org/10.1016/j.meatsci.2019.108039

Daugaard, M., Rohde, M., & Jäättelä, M. (2007). The heat shock protein 70 family: Highly homologous proteins with overlapping and distinct functions. *FEBS Letters*, *581*, 3702–3710. https://doi.org/https://doi.org/10.1016/j.febslet.2007.05.039

de Andrade, T. S., Albertini, T. Z., Barioni, L. G., de Medeiros, S. R., Millen, D. D., Dos Santos, A. C. R., ... & Lanna, D. P. D. (2020). Perception of consultants, feedlot owners, and packers regarding the optimal economic slaughter endpoint in feedlots: a national survey in Brazil (Part I). *Canadian Journal of Animal Science*, *100*(4), 745-758. https://doi.org/10.1139/cjas-2019-0219

Elahian, F., Sepehrizadeh, Z., Moghimi, B., & Abbas, S. (2014). Critical Reviews in Biotechnology Human cytochrome b5 reductase: structure, function, and potential applications. *Critical Reviews in Biotechnology*, *34*(2), 134–143. https://doi.org/10.3109/07388551.2012.732031

England, E. M., Matarneh, S. K., Scheffler, T. L., Wachet, C., & Gerrard, D. E. (2015). Altered AMP deaminase activity may extend postmortem glycolysis. *Meat Science*, *102*, 8–14. https://doi.org/10.1016/j.meatsci.2014.11.009

England, E. M., Matarneh, S. K., Oliver, E. M., Apaoblaza, A., Scheffler, T. L., Shi, H., & Gerrard, D. E. (2016). Excess glycogen does not resolve high ultimate pH of oxidative muscle. *Meat Science*, *114*, 95–102. https://doi.org/10.1016/j.meatsci.2015.10.010

Ertbjerg, P. (2022). Current understanding on the role of proteolysis on meat quality. In *New Aspects of Meat Quality: From Genes to Ethics, Second Edition* (pp. 95–114). Elsevier Ltd. https://doi.org/10.1016/B978-0-323-85879-3.00022-2

Ferraz, J. B. S., & de Felício, P. E. (2010). Production systems–An example from Brazil. *Meat science*, *84*(2), 238-243. https://doi.org/10.1016/j.meatsci.2009.06.006

Franco, D., Mato, A., Salgado, F. J., López-Pedrouso, M., Carrera, M., Bravo, S., … Zapata, C. (2015). Tackling proteome changes in the longissimus thoracis bovine muscle in response to pre-slaughter stress. *Journal of Proteomics*, *122*, 73–85. https://doi.org/10.1016/j.jprot.2015.03.029

Fuente-Garcia, C., Aldai, N., Sentandreu, E., Oliván, M., García-Torres, S., Franco, D., … Sentandreu, M. A. (2019). Search for proteomic biomarkers related to bovine pre-slaughter stress using liquid isoelectric focusing (OFFGEL) and mass spectrometry. *Journal of Proteomics*, *198*, 59–65. https://doi.org/10.1016/j.jprot.2018.10.013

Fuente-Garcia, C., Sentandreu, E., Aldai, N., Oliván, M., Ángel, M., & Sentandreu. (2020). Characterization of the myofibrillar proteome as a way to better understand differences in bovine meats having different ultimate pH values. *Proteomics*, *20*(12), 2000012. https://doi.org/https://doi.org/10.1002/pmic.202000012

Gagaoua, M., Monteils, V., & Picard, B. (2018a). Data from the farmgate-to-meat continuum including omics-based biomarkers to better understand the variability of beef tenderness: An integromics approach. *J Agric Food Chem*, *66*(51), 13552–13563. doi: 10.1021/acs.jafc.8b05744

Gagaoua, M., Bonnet, M., & Picard, B. (2020). Protein Array-Based Approach to Evaluate Biomarkers of Beef Tenderness and Marbling in Cows: Understanding of the Underlying Mechanisms and Prediction. *Foods*, *9*(9), 1180. https://doi.org/10.3390/foods9091180

Gagaoua, M., Bonnet, M., Ellies-Oury, M.-P., Koning, L. De, & Picard, B. (2018b). Reverse phase protein arrays for the identification/validation of biomarkers of beef texture and their use for early classification of carcasses. *Food Chemistry*, *250*, 245–252. https://doi.org/10.1016/j.foodchem.2018.01.070

Gagaoua, M., Terlouw, E. M. C., Boudjellal, A., & Picard, B. (2015). Coherent correlation networks among protein biomarkers of beef tenderness: What they reveal. *Journal of Proteomics*, *128*, 365–374. https://doi.org/10.1016/j.jprot.2015.08.022

Gagaoua, M., Hafid, K., Boudida, Y., Becila, S., Ouali, A., Picard, B., & Boudjellal, A. (2015). Caspases and Thrombin Activity Regulation by Specific Serpin Inhibitors in Bovine Skeletal Muscle. *Appl Biochem Biotechnol*, *177*, 279–303. https://doi.org/https://doi.org/10.1007/s12010-015-1762-4

Gagaoua, M., Hughes, J., Terlouw, E. M. C., Warner, R. D., Purslow, P. P., Lorenzo, J. M., & Picard, B. (2020). Trends in Food Science & Technology Proteomic biomarkers of beef colour. *Trends in Food Science & Technology*, *101*, 234–252. https://doi.org/10.1016/j.tifs.2020.05.005

Gagaoua, M., Schilling, W. M., Zhang, X., & Suman, S. P. (2022). *Applications of proteomics in meat research*. *Reference Module in Food Science* (Third Edit). Elsevier. https://doi.org/https://doi.org/10.1016/B978-0-323-85125-1.00123-X

Gagaoua, M., Terlouw, E. M. C., Richardson, I., Hocquette, J.-F., & Picard, B. (2019). The associations between proteomic biomarkers and beef tenderness depend on the end-point cooking temperature, the country origin of the panelists and breed. *Meat Science*, *157*, 107871. https://doi.org/10.1016/j.meatsci.2019.06.007

Gagaoua, M., Terlouw, E. M. C., Micol, D., Boudjellal, A., Hocquette, J.-F., & Picard, B. (2015). Understanding Early Post-Mortem Biochemical Processes Underlying Meat Color and pH Decline in the Longissimus thoracis Muscle of Young Blond d ' Aquitaine Bulls Using Protein Biomarkers. *Journal of Agricultural and Food Chemistry*, *63*, 6799–6809. https://doi.org/10.1021/acs.jafc.5b02615

Gagaoua, M., Terlouw, E. M. C., Mullen, A. M., Franco, D., Warner, R. D., Lorenzo, J. M., … Picard, B. (2021). Molecular signatures of beef tenderness : Underlying mechanisms based on integromics of protein biomarkers from multi-platform proteomics studies. *Meat Science*, *172*, 108311. https://doi.org/10.1016/j.meatsci.2020.108311

Gagaoua, M., Terlouw, E. M. C., & Picard, B. (2017). The study of protein biomarkers to understand the biochemical processes underlying beef color development in young bulls. *Meat Science*, *134*, 18–27. https://doi.org/10.1016/j.meatsci.2017.07.014

Gagaoua, M., Troy, D., & Mullen, A. M. (2021). The Extent and Rate of the Appearance of the Major 110 and 30 kDa Proteolytic Fragments during Post-Mortem Aging of Beef Depend on the Glycolysing Rate of the Muscle and Aging Time: An LC − MS/ MS Approach to Decipher Their Proteome and Associated Pathway. *Journal of Agricultural and Food Chemistry*, *69*, 602–614. https://doi.org/https://doi.org/10.1021/acs.jafc.0c06485

Gagaoua, M., Warner, R. D., Purslow, P., Ramanathan, R., Mullen, A. M., López-Pedrouso, M., … Terlouw, E. M. C. (2021). Dark-cutting beef: A brief review and an integromics meta-analysis at the proteome level to decipher the underlying pathways. *Meat Science*, *181*, 108611. https://doi.org/10.1016/j.meatsci.2021.108611

Gagaoua, M., Franco, D., & Ramanathan, R. (2024). Meat Omics: Trends and applications of Omics strategies in meat research. *J Proteomics*, *295*, 105090. https://doi.org/10.1016/j.jprot.2024.105090

García-Torres, S., Cabeza de Vaca, M., Tejerina, D., Romero-Fernández, M. P., Ortiz, A., Franco, D., … Oliván, M. (2021). Assessment of stress by serum biomarkers in calves and

their relationship to ultimate ph as an indicator of meat quality. *Animals*, *11*, 2291. https://doi.org/10.3390/ani11082291

Giorgi, C., Bonora, M., Sorrentino, G., Missiroli, S., Poletti, F., Suski, J. M., … Pinton, P. (2015). p53 at the endoplasmic reticulum regulates apoptosis in a Ca2 + -dependent manner. *PNAS*, *112*(6), 1779–1784. https://doi.org/10.1073/pnas.1410723112

Gómez, J. F. M., Cônsolo, N. R. B., Antonelo, D. S., Beline, M., Gagaoua, M., Higuera-Padilla, A., … Silva, S. L. (2022). Impact of Cattle Feeding Strategy on the Beef Metabolome. *Metabolites*, *12*, 640. https://doi.org/10.3390/metabo12070640

Green, D. R., Galluzzi, L., & Kroemer, G. (2014). Metabolic control of cell death. *Science*, *345*(6203). https://doi.org/10.1126/science.1250256

Hughes, J., Clarke, F., Li, Y., Purslow, P., & Warner, R. (2019). Differences in light scattering between pale and dark beef longissimus thoracis muscles are primarily caused by differences in the myofilament lattice, myofibril and muscle fibre transverse spacings. *Meat Science*, *149*, 96–106. https://doi.org/https://doi.org/10.1016/j.meatsci.2018.11.006

Hughes, J. M., Clarke, F. M., Purslow, P. P., & Warner, R. D. (2019). Meat color is determined not only by chromatic heme pigments but also by the physical structure and achromatic light scattering properties of the muscle. *Comprehensive Reviews in Food Science and Food Safety*, 1–20. https://doi.org/10.1111/1541-4337.12509

Ishii, H., Shirai, T., Makino, C., & Nishikata, T. (2014). Mitochondrial inhibitor sodium azide inhibits the reorganization of mitochondria-rich cytoplasm and the establishment of the anteroposterior axis in ascidian embryo. *Development, Growth & Differentiation*, *56*, 175–188. https://doi.org/10.1111/dgd.12117

Jiang, B., Liang, P., Deng, G., Tu, Z., Liu, M., & Xiao, X. (2011). Increased stability of Bcl-2 in HSP70-mediated protection against apoptosis induced by oxidative stress. *Cell Stress and Chaperones*, *16*, 143–152. https://doi.org/10.1007/s12192-010-0226-6

Kiyimba, F., Hartson, S. D., Rogers, J., Vanoverbeke, D. L., Mafi, G. G., & Ramanathan, R. (2022). Dark-cutting beef mitochondrial proteomic signatures reveal increased biogenesis proteins and bioenergetics capabilities. *Journal of Proteomics*, *265*, 104637. https://doi.org/10.1016/j.jprot.2022.104637

Kiyimba, F., Hartson, S. D., Rogers, J., VanOverbeke, D. L., Mafi, G. G., & Ramanathan, R. (2021). Changes in glycolytic and mitochondrial protein profiles regulates postmortem muscle acidification and oxygen consumption in dark-cutting beef. *Journal of Proteomics*, *232*, 104016. https://doi.org/10.1016/j.jprot.2020.104016

Kiyimba, F., Cassens, D., Hartson, S. D., Rogers, J., Habiger, J., Mafi, G. G., & Ramanathan, R. (2023). Integrative proteomics and metabolomics profiling to understand the biochemical basis of beef muscle darkening at a slightly elevated pH. *Journal of Animal Science*, *101*, skac376. https://doi.org/10.1093/jas/skac376

Lamri, M., della Malva, A., Djenane, D., Albenzio, M., & Gagaoua, M. (2023). First insights into the dynamic protein changes in goat Semitendinosus muscle during the post-mortem period using high-throughput proteomics. *Meat Science*, *202*, 109207. https://doi.org/10.1016/j.meatsci.2023.109207

Lamri, M., della Malva, A., Djenane, D., López-Pedrouso, M., Franco, D., Albenzio, M., … Gagaoua, M. (2023). Towards the discovery of goat meat quality biomarkers using label-free proteomics. *Journal of Proteomics*, *278*, 104868. https://doi.org/10.1016/j.jprot.2023.104868

Lee, S. M., Kim, J. H., Cho, E. J., & Youn, H. D. (2009). A nucleocytoplasmic malate dehydrogenase regulates p53 transcriptional activity in response to metabolic stress. *Cell Death and Differentiation*, *16*, 738–748. https://doi.org/10.1038/cdd.2009.5

Lek, M., Quinlan, K. G. R., & North, K. N. (2009). The evolution of skeletal muscle performance: gene duplication and divergence of human sarcomeric a-actinins. *BioEssays*, *32*, 17–25. https://doi.org/https://doi.org/10.1002/bies.200900110

Lièvremont, J.-P., Rizzuto, R., Hendershot, L., & Meldolesi, J. (1997). BiP, a Major Chaperone Protein of the Endoplasmic Reticulum Lumen, Plays a Direct and Important Role in the Storage of the Rapidly Exchanging Pool of Ca2+. *The Journal of Biological Chemistry*, *272*(49), 30873–30879. https://doi.org/10.1074/jbc.272.49.30873

Lomiwes, D., Farouk, M. M., Wu, G., & Young, O. A. (2014). The development of meat tenderness is likely to be compartmentalised by ultimate pH. *Meat Science*, *96*, 646–651. https://doi.org/10.1016/j.meatsci.2013.08.022

Longo, V., Lana, A., Bottero, M. T., & Zolla, L. (2015). Apoptosis in muscle-to-meat aging process: The omic witness. *Journal of Proteomics*, *125*, 29–40. https://doi.org/10.1016/J.JPROT.2015.04.023

López-Pedrouso, M., Lorenzo, J. M., Cittadini, A., Sarries, M. V, Gagaoua, M., & Franco, D. (2022). A proteomic approach to identify biomarkers of foal meat quality: A focus on tenderness, color and intramuscular fat traits. *Food Chemistry Journal*, *405*, 134805. https://doi.org/10.1016/j.foodchem.2022.134805

Mahmood, S., Turchinsky, N., Paradis, F., Dixon, W. T., & Bruce, H. L. (2018). Proteomics of dark cutting longissimus thoracis muscle from heifer and steer. *Meat Science*, *137*, 47–57. https://doi.org/10.1016/j.meatsci.2017.11.014

Malheiros, J. M., Enriquez-Valencia, C. E., Silva, J. A. I. de V., Curi, R. A., de Oliveira, H. N., de Albuquerque, L. G., & Chardulo, L. A. L. (2020). Carcass and meat quality of Nellore cattle (Bos taurus indicus) belonging to the breeding programs. *Livestock Science*, *242*, 104277. https://doi.org/10.1016/j.livsci.2020.104277

Matarneh, S. K., Beline, M., Luz, S. De, Shi, H., & Gerrard, D. E. (2018). Mitochondrial F1-ATPase extends glycolysis and pH decline in an in vitro model. *Meat Science*, *137*, 85–91. https://doi.org/10.1016/j.meatsci.2017.11.009

Matarneh, S. K., England, E. M., Scheffler, T. L., Yen, C. N., Wicks, J. C., Shi, H., & Gerrard, D. E. (2017). A mitochondrial protein increases glycolytic flux. *Meat Science*, *133*, 119–125. https://doi.org/10.1016/j.meatsci.2017.06.007

Matarneh, S. K., Yen, C., Bodmer, J., El-kadi, S. W., & Gerrard, D. E. (2021). Mitochondria influence glycolytic and tricarboxylic acid cycle metabolism under postmortem simulating conditions. *Meat Science*, *172*, 108316. https://doi.org/10.1016/j.meatsci.2020.108316

Mato, A., Rodríguez-Vázquez, R., López-Pedrouso, M., Bravo, S., Franco, D., & Zapata, C. (2019). The first evidence of global meat phosphoproteome changes in response to pre-slaughter stress. *BMC Genomics*, *20*(590). https://doi.org/https://doi.org/10.1186/s12864-019-5943-3

Ojima, K., Kawabata, Y., Nakao, H., Nakao, K., Doi, N., Kitamura, F., … Kawahara, H. (2010). Dynamic distribution of muscle-specific calpain in mice has a key role in physical-stress adaptation and is impaired in muscular dystrophy. *The Journal of Clinical Investigation*, *120*(8). https://doi.org/10.1172/JCI40658.2672

Okamoto, K., Matsuzaka, Y., Yoshikawa, Y., Takaki, A., Kulski, J. K., Tamiya, G., & Inoko, H. (2003). Identification of NAD+ -dependent isocitrate dehydrogenase 3 γ-like (IDH3GL) gene and its genetic polymorphisms. *Gene*, *323*, 141–148. https://doi.org/10.1016/j.gene.2003.09.014

Ouali, A., Gagaoua, M., Boudida, Y., Becila, S., Boudjellal, A., Herrera-mendez, C. H., & Sentandreu, M. A. (2013). Biomarkers of meat tenderness: Present knowledge and perspectives in regards to our current understanding of the mechanisms involved. *Meat Science*, *95*, 854–870. https://doi.org/10.1016/j.meatsci.2013.05.010

Pescador, N., Villar, D., Cifuentes, D., Garcia-Rocha, M., Ortiz-Barahona, A., Vazquez, S., … Peso, L. del. (2010). Hypoxia Promotes Glycogen Accumulation through Hypoxia Inducible Factor (HIF)-Mediated Induction of Glycogen Synthase 1. *PLoS One*, *5*(3), e9644. https://doi.org/10.1371/journal.pone.0009644

Patinho, I., Cavalcante, C.L., Saldaña, E., Gagaoua, M., Behrens, G.H. & Contreras-Castillo, C.J. (2024). Assessment of beef sensory attributes and physicochemical characteristics: A comparative study of intermediate versus normal ultimate pH striploin cuts. *Food Research International*, 175, 113778. https://doi.org/10.1016/j.foodres.2023.113778

Picard, B., & Gagaoua, M. (2017). Proteomic Investigations of Beef Tenderness. *Proteomics in Food Science*. Elsevier Inc. https://doi.org/10.1016/B978-0-12-804007-2.00011-4

Picard, B., & Gagaoua, M. (2020). Meta-proteomics for the discovery of protein biomarkers of beef tenderness: An overview of integrated studies. *Food Research International*, *127*, 108739. https://doi.org/10.1016/j.foodres.2019.108739

Pillar, N., Pleniceanu, O., Fang, M., Ziv, L., Lahav, E., Botchan, S., … Dekel, B. (2017). A rare variant in the FHL1 gene associated with X‐linked recessive hypoparathyroidism. *Human Genetics*, *136*, 835–845. https://doi.org/10.1007/s00439-017-1804-9

Poleti, M. D., Moncau, C. T., Silva-Vignato, B., Rosa, A. F., Lobo, A. R., Cataldi, T. R., … de Carvalho Balieiro, J. C. (2018). Label-free quantitative proteomic analysis reveals muscle contraction and metabolism proteins linked to ultimate pH in bovine skeletal muscle. *Meat Science*, *145*, 209–219. https://doi.org/10.1016/j.meatsci.2018.06.041

Ponnampalam, E. N., Hopkins, D. L., Bruce, H., Li, D., Baldi, G., & Bekhit, A. E. (2017). Causes and Contributing Factors to "Dark Cutting" Meat: Current Trends and Future Directions: A Review. *Comprehensive Reviews in Food Science and Food Safety*, *16*(3), 400–430. https://doi.org/10.1111/1541-4337.12258

Purslow, P. P., Gagaoua, M., & Warner, R. D. (2021). Insights on meat quality from combining

traditional studies and proteomics. *Meat Science*, *174*, 108423. https://doi.org/10.1016/j.meatsci.2020.108423

Rodrigues, R. T. D. S., Chizzotti, M. L., Vital, C. E., Baracat-Pereira, M. C., Barros, E., Busato, K. C., … Martins, T. D. S. (2017). Differences in beef quality between Angus (Bos taurus taurus) and Nellore (Bos taurus indicus) cattle through a proteomic and phosphoproteomic approach. *PLoS ONE*, *12*(1), 1–21. https://doi.org/10.1371/journal.pone.0170294

Schulte, M. D., Hochmuth, K. G., Steadham, E. M., Lonergan, S. M., Hansen, S. L., & Huff-lonergan, E. J. (2022). Early postmortem muscle proteome and metabolome of beef longissimus thoracis muscle classified by pH at 6 hours postmortem. *Journal of Proteomics*, *271*, 104756. https://doi.org/https://doi.org/10.1016/j.jprot.2022.104756

Sedoris, K. C., Thomas, S. D., & Miller, D. M. (2010). Hypoxia induces differential translation of enolase / MBP-1. *BMC Cancer*, *10*(157). https://doi.org/https://doi.org/10.1186/1471-2407-10-157

Sentandreu, E., Fuente-García, C., Pardo, O., Oliván, M., León, N., Aldai, N., … Sentandreu, M. A. (2021). Protein Biomarkers of Bovine Defective Meats at a Glance: Gel-Free Hybrid Quadrupole-Orbitrap Analysis for Rapid Screening. *Journal of Agricultural and Food Chemistry*, *69*, 7478–7487. https://doi.org/10.1021/acs.jafc.1c02016

Shathasivam, T., Kislinger, T., & Gramolini, A. O. (2010). Genes, proteins and complexes: the multifaceted nature of FHL family proteins in diverse tissues. *Journal of Cellular and Molecular Medicine*, *14*(12), 2702–2720. https://doi.org/10.1111/j.1582-4934.2010.01176.x

Shen, Q. W., Gerrard, D. E., & Du, M. (2008). Compound C , an inhibitor of AMP-activated protein kinase , inhibits glycolysis in mouse longissimus dorsi postmortem. *Meat Science*, *78*, 323–330. https://doi.org/10.1016/j.meatsci.2007.06.023

Shojapour, M., Fatemi, F., Farahmand, S., & Shasaltaneh, M. D. (2021). Investigation of Cyc1 protein structure stability after H53I mutation using computational approaches to improve redox potential. *Journal of Molecular Graphics and Modelling*, *105*, 107864. https://doi.org/10.1016/j.jmgm.2021.107864

Sierra, V., González-Blanco, L., Diñeiro, Y., Díaz, F., García-Espina, M. J., Coto-Montes, A., … Oliván, M. (2021). New Insights on the Impact of Cattle Handling on Post-Mortem Myofibrillar Muscle Proteome and Meat Tenderization. *Foods*, *10*, 3115. https://doi.org/https://doi.org/10.3390/foods10123115

Stambergova, H., Skarydova, L., Dunford, J. E., & Wsol, V. (2014). Biochemical properties of human dehydrogenase/reductase (SDR family) member 7. *Chemico-Biological Interactions Journal*, *207*, 52–57. https://doi.org/10.1016/j.cbi.2013.11.003

Suman, S. P., & Joseph, P. (2013). Myoglobin chemistry and meat color. *Annual Review of Food Science and Technology*, *4*, 79–99. https://doi.org/10.1146/annurev-food-030212-182623

Suman, S. P., Wang, Y., Gagaoua, M., Kiyimba, F., & Ramanathan, R. (2023). Proteomic approaches to characterize biochemistry of fresh beef color. *Journal of Proteomics*, *281*, 104893. https://doi.org/10.1016/j.jprot.2023.104893

Tang, J., Faustman, C., Hoagland, T. A., Mancini, R. A., Seyfert, M., & Hunt, M. (2005).

Postmortem Oxygen Consumption by Mitochondria and Its Effects on Myoglobin Form and Stability. *Journal of Agricultural and Food Chemistry*, *53*, 1223−1230. https://doi.org/10.1021/jf048646o

Tarrant, P. V. (1989). Animal Behaviour and Environment in the Dark-Cutting Condition in Beef - A Review. *Irish Journal of Food Science and Technology*, *13*(1), 1–21. https://doi.org/http://www.jstor.org/stable/25580937

Tasdemir, E., Maiuri, M. C., Galluzzi, L., Vitale, I., Djavaheri-mergny, M., Amelio, M. D., … Blomgren, K. (2008). Regulation of autophagy by cytoplasmic p53. *Nature Cell Biology*, *10*(6), 676–687. https://doi.org/https://doi.org/10.1038/ncb1730

Terlouw, E. M. C., Picard, B., Deiss, V., Berri, C., Hocquette, J. F., Lebret, B., … Gagaoua, M. (2021). Understanding the determination of meat quality using biochemical characteristics of the muscle: Stress at slaughter and other missing keys. *Foods*, *10*, 84. https://doi.org/10.3390/foods10010084

Ubaida-Mohien, C., Lyashkov, A., Gonzalez-freire, M., Tharakan, R., Shardell, M., Moaddel, R., … Ferrucci, L. (2019). Discovery proteomics in aging human skeletal muscle finds change in spliceosome, immunity, proteostasis and mitochondria. *ELife*, *8*(e49874). https://doi.org/DOI: https://doi.org/10.7554/eLife.49874.001

Wiedemann, N., Frazier, A. E., & Pfanner, N. (2004). The Protein Import Machinery of Mitochondria. *Journal of Biological Chemistry*, *279*(15), 14473–14476. https://doi.org/https://doi.org/10.1074/jbc.R400003200

Wu, S., Luo, X., Yang, X., Hopkins, D. L., Mao, Y., & Zhang, Y. (2020). Understanding the development of color and color stability of dark cutting beef based on mitochondrial proteomics. *Meat Science*, *163*, 108046. https://doi.org/10.1016/j.meatsci.2020.108046

Wu, W., Gao, X., Dai, Y., Fu, Y., Li, X., & Dai, R. (2015). Post-mortem changes in sarcoplasmic proteome and its relationship to meat color traits in M. semitendinosus of Chinese Luxi yellow cattle. *Food Research International*, *72*, 98–105. https://doi.org/10.1016/j.foodres.2015.03.030

Wulff, T., Jokumsen, A., Højrup, P., & Jessen, F. (2012). Time-dependent changes in protein expression in rainbow trout muscle following hypoxia. *Journal of Proteomics*, *75*, 2342–2351. https://doi.org/10.1016/j.jprot.2012.02.010

Yang, X., Wu, S., Hopkins, D. L., Liang, R., Zhu, L., & Zhang, Y. (2018). Proteomic analysis to investigate color changes of chilled beef longissimus steaks held under carbon monoxide and high oxygen packaging. *Meat Science*, *142*, 23–31. https://doi.org/10.1016/j.meatsci.2018.04.001

Yu, Q., Wu, W., Tian, X., Jia, F., Xu, L., Dai, R., & Li, X. (2017). Comparative proteomics to reveal muscle-specific beef color stability of Holstein cattle during post-mortem storage. *Food Chemistry*, *229*, 769–778. https://doi.org/10.1016/j.foodchem.2017.03.004

Zhai, C., Djimsa, B. A., Prenni, J. E., Woerner, D. R., & Belk, K. E. (2020). Tandem mass tag labeling to characterize muscle-specific proteome changes in beef during early postmortem period. *Journal of Proteomics*, *222*, 103794. https://doi.org/10.1016/j.jprot.2020.103794

Zhao, Y., Kong, X., Yang, X., Zhu, L., Liang, R., Luo, X., … Zhang, Y. (2022). Effect of energy metabolism and proteolysis on the toughness of intermediate ultimate pH beef. *Meat Science*, *188*, 108798. https://doi.org/10.1016/j.meatsci.2022.108798

Zhu, Y., Gagaoua, M., Mullen, A. M., Kelly, A. L., Sweeney, T., Cafferky, J., … Hamill, R. M. (2021). A Proteomic Study for the Discovery of Beef Tenderness Biomarkers and Prediction of Warner–Bratzler Shear Force Measured on Longissimus thoracis Muscles of Young Limousin-Sired Bulls. *Foods*, *10*, 952. https://doi.org/10.3390/foods10050952

Figure captions

Fig. 1. pH declines of the carcasses used in this trial. **A)** Individual pH decline curves of the carcasses, which are further depicted with the average curves comparing the normal (n = 5) and high (n = 5) pH groups. The blue and red lines indicate the pH values of pH 6.0 and pH 5.8 on which the meat can be considered dark-cutting meat at 48h *postmortem*. **B)** ANOVA analysis comparing the pH values over *postmortem* times between normal and high pH groups. (Significance: ns: not significant, $**P < 0.01$; $***P < 0.001$).

Fig. 2. Principal component analysis (PCA). **A)** First principal components (axis) depicting the relationships among the meat quality traits: pH traits over *postmortem* times, color traits, shear force and cook loss, all evaluated at 72h *postmortem*. **B)** Bi-plot highlighting the extent of separation of the carcasses from high and normal pH groups. **C)** Individual and overall Kaiser-Meyer-Olkin (KMO) computed for the PCA.

Fig. 3. Differentially abundant proteins (DAPs) between high and normal ultimate pH (pHu) beef at 30 min *postmortem*. **A)** Volcano plot showing the proteins significantly different (fold change ≥ 1.2 and *P*-value ≤ 0.05) between high and normal pHu beef at 30 min *postmortem*. The up- and down-regulated proteins from high *versus* normal pHu beef are shown in red and blue, respectively (details on the full names of the proteins are given in **Table 2**). **B)** Functional enrichment analysis using Metascape®. The top 12 enriched and significant terms ranked by their p-value are given. Stronger colors represent greater significant enrichment. Functional enrichment was performed by selecting gene ontology (GO) Biological Processes, GO Molecular Function, Reactome gene sets, and KEGG pathway as ontology sources. **C)** Functional enrichment network using Metascape®. Each enriched cluster term is presented with the corresponding color, where nodes that share the same cluster ID are typically close to each other. The sizes of the nodes reflect the enrichment significance of the terms. **D)** Protein-protein interaction analysis of the 33 DAPs using STRING database clustered into molecular functions and biological pathways using manual annotations. **E)** Hierarchical heatmap clustering to compare the enriched GO terms within the up- and down-regulated proteins. The heatmap colored by the p-values are indicated by color, where grey cells indicate a lack of significant enrichment in that GO, palest brown indicates a low p-value and darkest brown indicates a high p-value in each of the corresponding pHu class. The statistics details of each enriched term are given in **Table S1**.

Fig. 4. Differentially abundant proteins (DAPs) between high and normal ultimate pH (pHu) beef at 9 h *postmortem*. **A)** Volcano plot showing the proteins significantly different (fold change ≥ 1.2 and *P*-value ≤ 0.05) between high and normal pHu beef at 9 h *postmortem*. The up- and down-regulated proteins from high *versus* normal pHu beef are shown in red and blue, respectively (details on the full names of the proteins are given in **Table 3**). **B)** Functional enrichment analysis using Metascape®. The top 20 enriched and significant terms ranked by their p-value are given. Stronger colors represent greater significant enrichment. Functional enrichment was performed by selecting gene ontology (GO) Biological Processes, GO Molecular Function, Reactome gene sets, and KEGG pathway as ontology sources. **C)** Functional enrichment network using Metascape®. Each enriched cluster term is presented with the corresponding color, where nodes that share the same cluster ID are typically close to each other. The sizes of the nodes reflect the enrichment significance of the terms. **D)** Protein-protein interaction analysis of the 181 DAPs using STRING database clustered into molecular functions and biological pathways using manual annotations. **E)** Hierarchical heatmap clustering to

compare the enriched GO terms within the up- and down-regulated proteins. The heatmap colored by the p-values are indicated by color, where grey cells indicate a lack of significant enrichment in that GO, palest brown indicates a low p-value and darkest brown indicates a high p-value in each of the corresponding pHu class. The statistics details of each enriched term are given in **Table S2**.

Fig. 5. Differentially abundant proteins (DAPs) between high and normal ultimate pH (pHu) beef at 44 h *postmortem*. **A)** Volcano plot showing the proteins significantly different (fold change ≥ 1.2 and *P*-value ≤ 0.05) between high and normal pHu beef at 44 h *postmortem*. The up- and down-regulated proteins from high *versus* normal pHu beef are shown in red and blue, respectively (details on the full names of the proteins are given in **Table 4**). **B)** Functional enrichment analysis using Metascape®. The top 19 enriched and significant terms ranked by their p-value are given. Stronger colors represent greater significant enrichment. Functional enrichment was performed by selecting gene ontology (GO) Biological Processes, GO Molecular Function, Reactome gene sets, and KEGG pathway as ontology sources. **C)** Functional enrichment network using Metascape®. Each enriched cluster term is presented with the corresponding color, where nodes that share the same cluster ID are typically close to each other. The sizes of the nodes reflect the enrichment significance of the terms. **D)** Protein-protein interaction analysis of the 37 DAPs using STRING database clustered into molecular functions and biological pathways using manual annotations. **E)** Hierarchical heatmap clustering to compare the enriched GO terms within the up- and down-regulated proteins. The heatmap colored by the p-values are indicated by color, where grey cells indicate a lack of significant enrichment in that GO, palest brown indicates a low p-value and darkest brown indicates a high p-value in each of the corresponding pHu class. The statistics details of each enriched term are given in **Table S3**.

Fig. 6. Biological pathway and process enrichment analysis on the total differentially abundant proteins (DAPs) proteins (n = 251) identified to change between high and normal ultimate pH (pHu) beef at 30 min, 9 h and 44 h *postmortem*. **A)** Circos plot depicting the overlap between proteins across the *postmortem* times. Twenty-three common proteins according to *postmortem* time comparison are given. **B)** Functional enrichment analysis of the 23 common proteins using Metascape®. The top 8 enriched and significant terms ranked by their p-value are given. Stronger colors represent greater significant enrichment. Functional enrichment was performed by selecting gene ontology (GO) Biological Processes, GO Molecular Function, Reactome gene sets, and KEGG pathway as ontology sources. **C)** Functional enrichment network using Metascape®. Each enriched cluster term is presented with the corresponding color, where nodes that share the same cluster ID are typically close to each other. The sizes of the nodes reflect the enrichment significance of the terms. **D)** Hierarchical clustering analysis built using the 23 common (DAPs) proteins given in the Circos plot. The heatmap shows the relative abundances of the proteins using only pH group/time averages. The details on the protein names that are up and down, refer to **Table 2**, **Table 3** and **Table 4**. **E)** Protein-protein interaction analysis of the 23 common proteins using STRING database clustered into molecular functions and biological pathways using manual annotations. **F)** Hierarchical heatmap clustering to compare the enriched GO terms within the *postmortem* time comparison. The heatmap colored by the p-values are indicated by color, where grey cells indicate a lack of significant enrichment in that GO, palest brown indicates a low p-value and darkest brown indicates a high p-value in each of the corresponding *postmortem* time.

Fig. 7. Secretome analysis. The secretome analyses have been performed for the 3 protein lists (30min, 9h and 44h). The proteins secreted through classical pathways or non-classical pathways are given. SERPINC1 depicted in gold character was a common secreted protein through classical pathways for both 9h and 44h *postmortem*.

Fig. 8. Biological pathway and process enrichment analysis on the total differentially abundant proteins (DAPs) proteins (n = 251) identified to change between high and normal ultimate pH (pHu) beef at 30 min, 9 h and 44 h *postmortem* in comparison with the dark-cutting database from Gagaoua et al. (2021). Circos plot depicting the overlap between proteins across the studies at 30 min (**A**), 9 h (**B**) and 44 h (**C**) *postmortem*. Each outside arc represents one study with a different color. On the inside, the dark orange color represents the proteins that appear in multiple lists and the light orange color represents proteins that are unique to that protein list; and purple lines link the same protein (gene name) that are shared by the input. The length of the outside arcs is related to the number of proteins in each list. Hierarchical Heatmap clustering indicating the first top 20 enriched gene ontology (GO) terms at 30 min (**D**), 9 h (**E**) and 44 h (**F**) *postmortem*. Functional enrichment was performed using Metascape® by selecting gene ontology (GO) Biological Processes, GO Molecular Function, Reactome gene sets, and KEGG pathway as ontology sources. The heatmap colored by the p-values are indicated by color, where grey cells indicate a lack of significant enrichment in that GO, palest brown indicates a low p-value and darkest brown indicates a high p-value in each of the corresponding study.

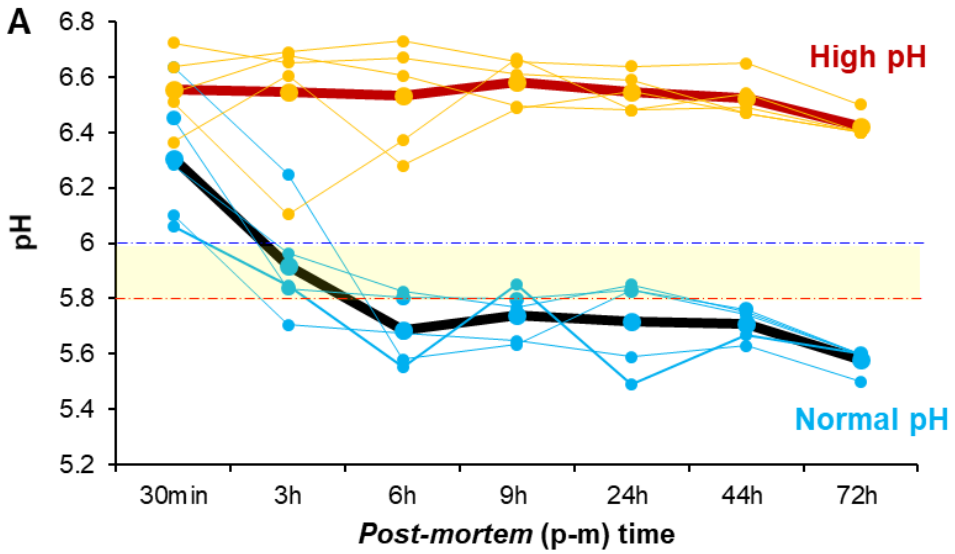

B

pH group \ p-m time	30min	3h	6h	9h	24h	44h	72h
High pH	6.56	6.55	6.53	6.58	6.55	6.52	6.42
Normal pH	6.31	5.92	5.69	5.74	5.72	5.71	5.58
SEM	0.07	0.12	0.15	0.14	0.14	0.14	0.14
Significance	ns	**	***	***	***	***	***

Fig. 1.

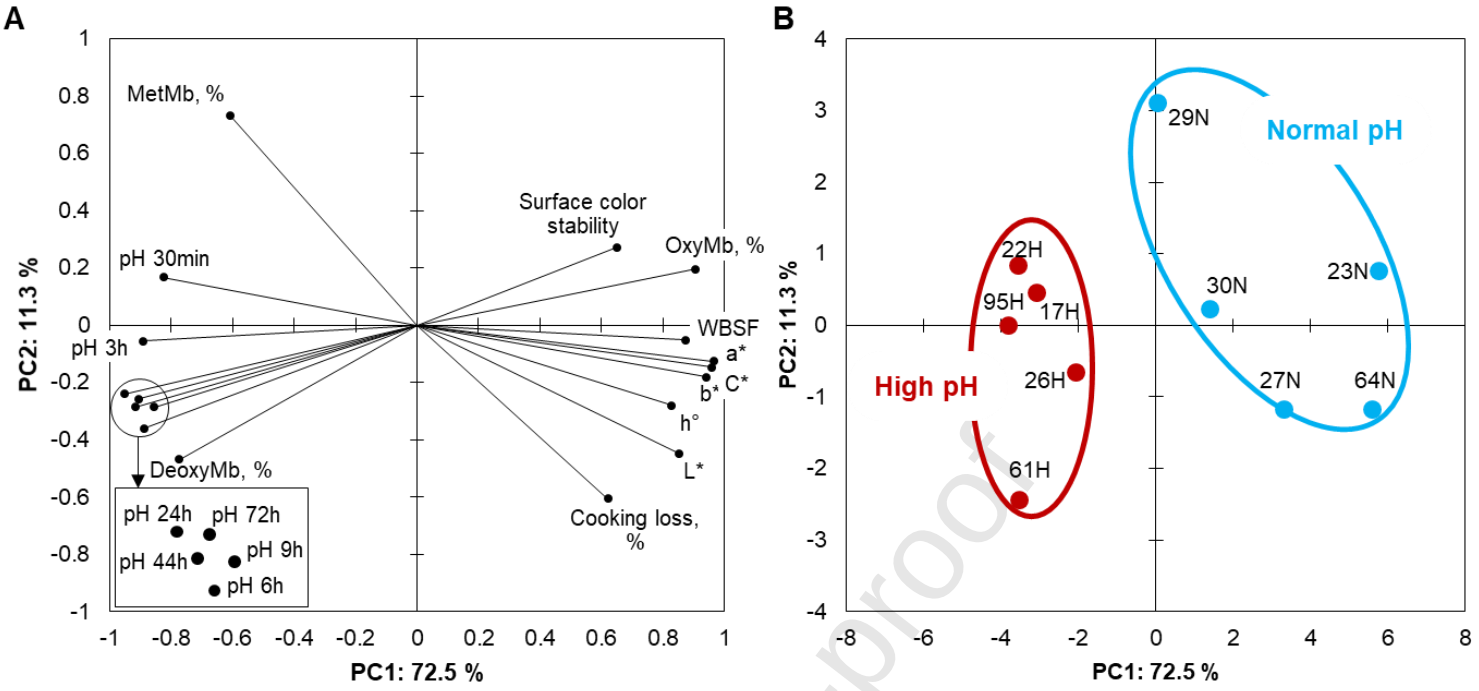

C

Variables	*L**	*a**	*b**	*C**	*h°*	MetMb, %	DeoxyMb, %	OxyMb, %	Surface color stability	Cooking loss, %	WBSF, N	pH 30min	pH 3h	pH 6h	pH 9h	pH 24h	pH 44h	pH 72h	Overall KMO
KMO values	0.64	0.72	0.81	0.73	0.66	0.63	0.72	0.79	0.62	0.49	0.68	0.83	0.81	0.69	0.76	0.65	0.62	0.70	**0.70**

Fig. 2.

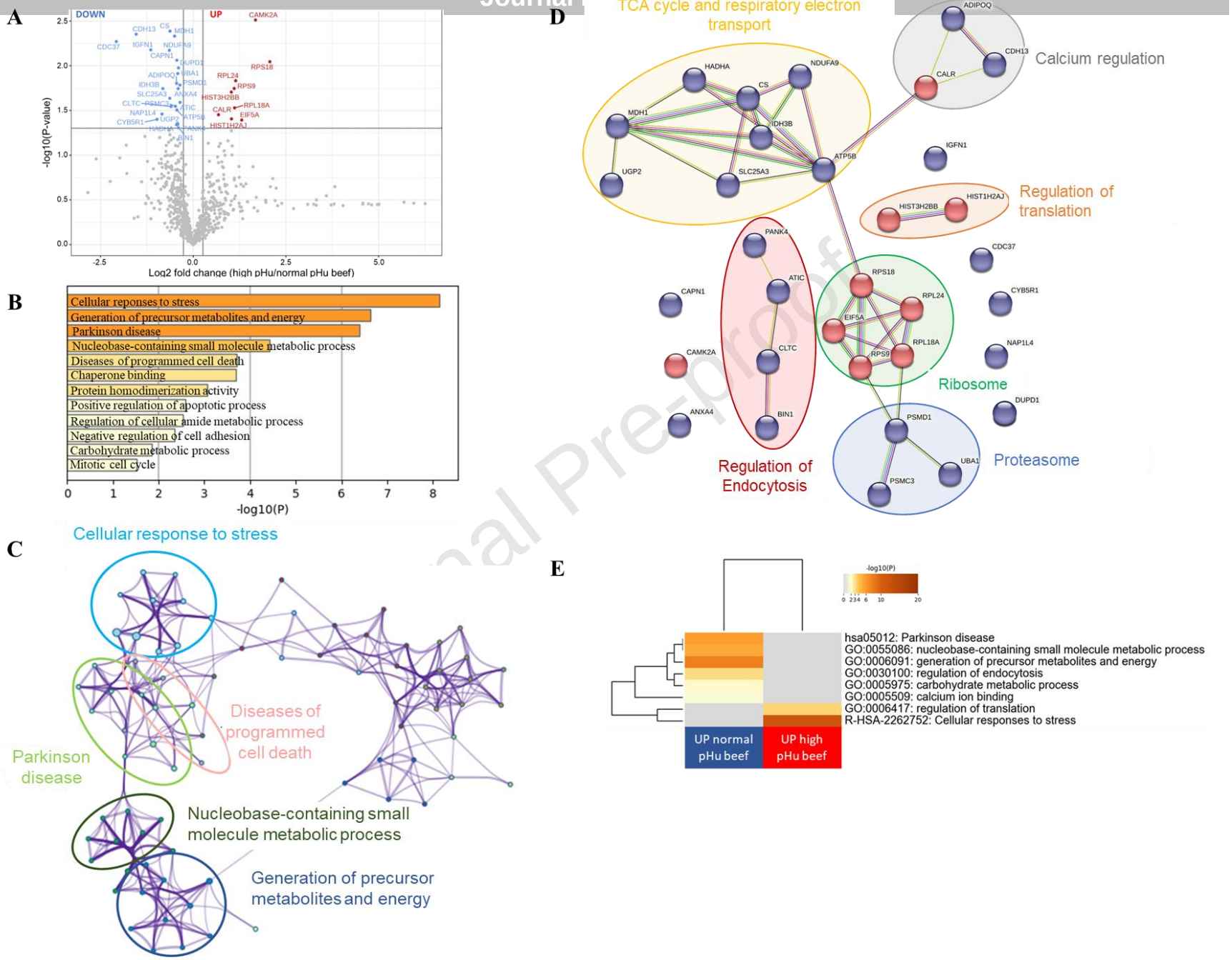

Fig. 3.

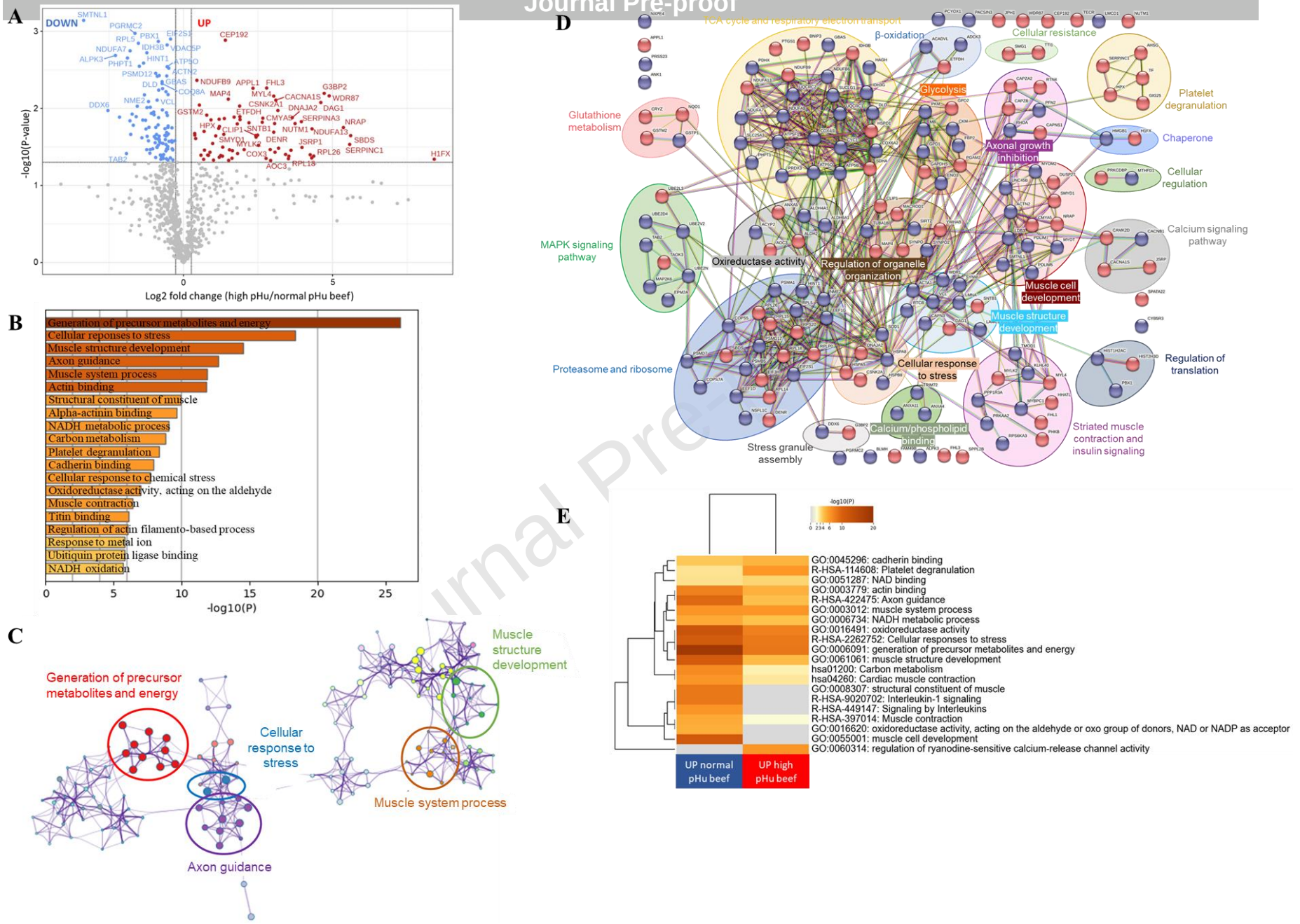

Fig. 4.

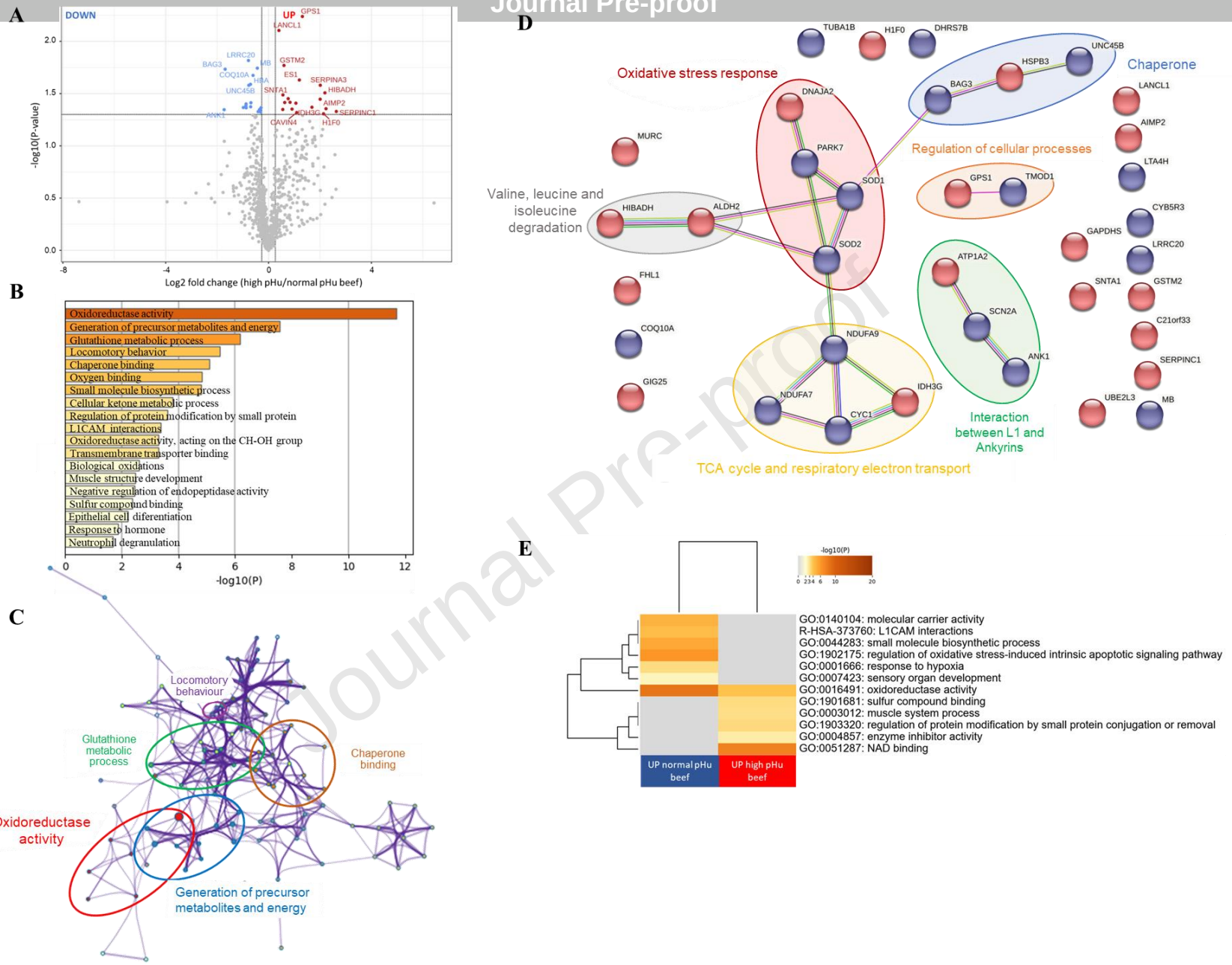

Fig. 5.

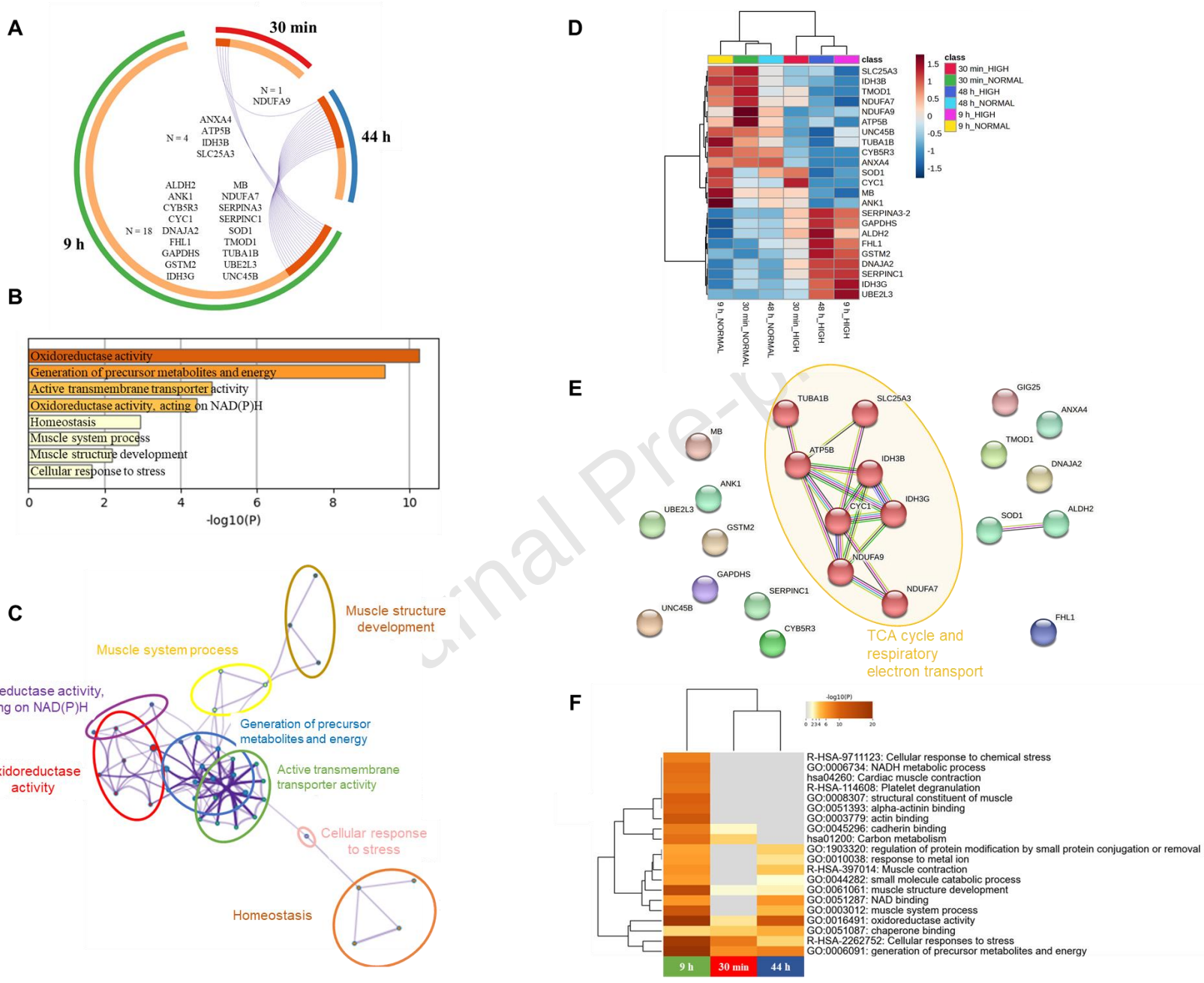
A
30 min
44 h
9 h
N = 1
NDUFA9
N = 4
ANXA4
ATP5B
IDH3B
SLC25A3
N = 18
ALDH2
ANK1
CYB5R3
CYC1
DNAJA2
FHL1
GAPDHS
GSTM2
IDH3G
MB
NDUFA7
SERPINA3
SERPINC1
SOD1
TMOD1
TUBA1B
UBE2L3
UNC45B
B
Oxidoreductase activity
Generation of precursor metabolites and energy
Active transmembrane transporter activity
Oxidoreductase activity, acting on NAD(P)H
Homeostasis
Muscle system process
Muscle structure development
Cellular response to stress
0
2
4
6
8
10
-log10(P)
C
Muscle structure development
Muscle system process
Oxidoreductase activity, acting on NAD(P)H
Generation of precursor metabolites and energy
Oxidoreductase activity
Active transmembrane transporter activity
Cellular response to stress
Homeostasis
D
class
SLC25A3
IDH3B
TMOD1
NDUFA7
NDUFA9
ATP5B
UNC45B
TUBA1B
CYB5R3
ANXA4
SOD1
CYC1
MB
ANK1
SERPINA3-2
GAPDHS
ALDH2
FHL1
GSTM2
DNAJA2
SERPINC1
IDH3G
UBE2L3
9 h_NORMAL
30 min_NORMAL
48 h_NORMAL
30 min_HIGH
48 h_HIGH
9 h_HIGH
1.5
1
0.5
0
-0.5
-1
-1.5
class
30 min_HIGH
30 min_NORMAL
48 h_HIGH
48 h_NORMAL
9 h_HIGH
9 h_NORMAL
E
TUBA1B
SLC25A3
MB
ATP5B
IDH3B
ANK1
UBE2L3
CYC1
IDH3G
GSTM2
NDUFA9
GAPDHS
NDUFA7
SERPINC1
UNC45B
CYB5R3
TCA cycle and respiratory electron transport
GIG25
ANXA4
TMOD1
DNAJA2
SOD1
ALDH2
FHL1
F
-log10(P)
0 2 3 4 6 10 20
R-HSA-9711123: Cellular response to chemical stress
GO:0006734: NADH metabolic process
hsa04260: Cardiac muscle contraction
R-HSA-114608: Platelet degranulation
GO:0008307: structural constituent of muscle
GO:0051393: alpha-actinin binding
GO:0003779: actin binding
GO:0045296: cadherin binding
hsa01200: Carbon metabolism
GO:1903320: regulation of protein modification by small protein conjugation or removal
GO:0010038: response to metal ion
R-HSA-397014: Muscle contraction
GO:0044282: small molecule catabolic process
GO:0061061: muscle structure development
GO:0051287: NAD binding
GO:0003012: muscle system process
GO:0016491: oxidoreductase activity
GO:0051087: chaperone binding
R-HSA-2262752: Cellular responses to stress
GO:0006091: generation of precursor metabolites and energy
9 h
30 min
44 h

Fig. 6.

pH group	Bovine Uniprot ID	Gene Name	Localizations	Signals	Cytoplasm	Nucleus	Extracellular	Cell membrane	Mitochondrion	Plastid	Endoplasmic reticulum	Lysosome / Vacuole	Golgi apparatus	Peroxisome	Secretion pathways
30 min	Q3Y5Z3	ADIPOQ	Extracellular	Signal peptide	0.20	0.13	0.94	0.20	0.07	0.00	0.16	0.27	0.14	0.00	Classical
	P52193	CALR	Extracellular | Endoplasmic reticulum	Signal peptide	0.23	0.09	0.69	0.19	0.07	0.01	0.78	0.30	0.35	0.03	
9H	F1MD77	LAMC1	Extracellular	Signal peptide	0.21	0.11	0.89	0.41	0.12	0.01	0.34	0.27	0.37	0.01	
	F1N184	NXPE4	Extracellular	Signal peptide	0.39	0.27	0.70	0.37	0.24	0.01	0.24	0.21	0.30	0.02	
	P12763	AHSG	Extracellular	Signal peptide	0.16	0.08	0.94	0.11	0.06	0.03	0.15	0.31	0.22	0.00	
	P41361	**SERPINC1**	Extracellular	Signal peptide	0.20	0.06	0.91	0.23	0.08	0.01	0.32	0.22	0.31	0.01	
	P81287	ANXA5	Cytoplasm | Extracellular | Lysosome/Vacuole	NaN	0.77	0.47	0.68	0.45	0.19	0.01	0.10	0.63	0.03	0.06	
	Q1LZE9	PRSS23	Extracellular	Signal peptide	0.11	0.08	0.93	0.28	0.08	0.01	0.18	0.19	0.13	0.02	
	Q29443	TF	Extracellular	Signal peptide	0.24	0.07	0.84	0.46	0.19	0.03	0.46	0.38	0.32	0.00	
	Q3SZV7	HPX	Extracellular	Signal peptide	0.20	0.12	0.89	0.27	0.24	0.00	0.30	0.42	0.37	0.01	
	F1MBP8	COPS5	Cytoplasm | Nucleus | Lysosome/Vacuole	Nuclear export signal	0.57	0.56	0.00	0.38	0.26	0.01	0.18	0.59	0.07	0.12	Non-classical
	O18738	DAG1	Cell membrane	Signal peptide | Transmembrane domain	0.18	0.12	0.40	0.79	0.06	0.01	0.16	0.38	0.26	0.02	
	F1N206	DLD	Mitochondrion	Mitochondrial transit peptide	0.14	0.11	0.07	0.07	0.91	0.10	0.04	0.03	0.06	0.03	
	P10103	HMGB1	Cytoplasm|Nucleus	Nuclear localization signal	0.53	0.73	0.38	0.24	0.14	0.01	0.08	0.05	0.12	0.02	
44h	P41361	**SERPINC1**	Extracellular	Signal peptide	0.20	0.06	0.91	0.23	0.08	0.01	0.32	0.22	0.31	0.01	Classical

Fig. 7.

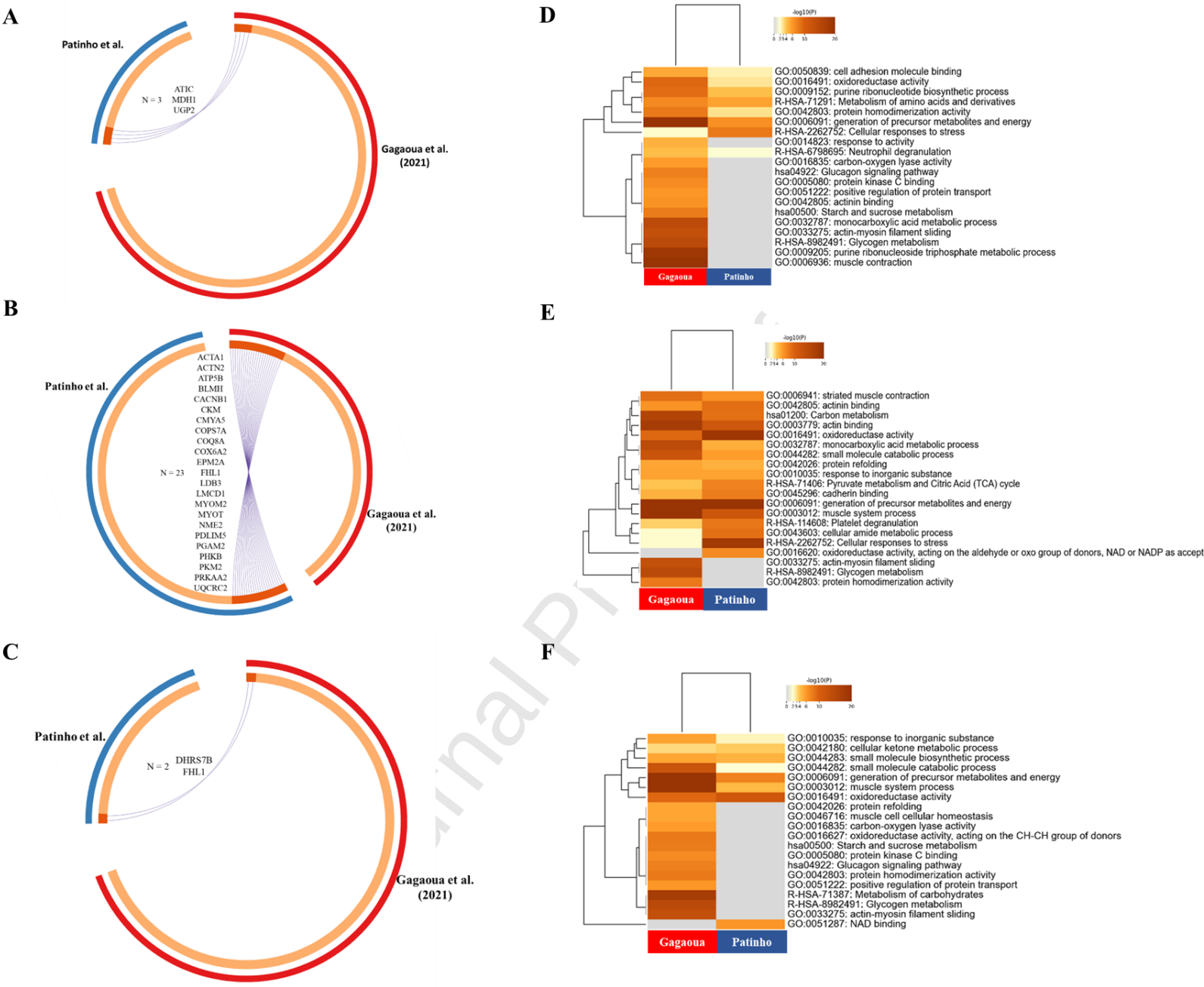
A
Patinho et al.
N = 3
ATIC
MDH1
UGP2
Gagaoua et al. (2021)
B
Patinho et al.
N = 23
ACTA1
ACTN2
ATP5B
BLMH
CACNB1
CKM
CMYA5
COPS7A
COQ8A
COX6A2
EPM2A
FHL1
LDB3
LMCD1
MYOM2
MYOT
NME2
PDLIM5
PGAM2
PHKB
PKM2
PRKAA2
UQCRC2
Gagaoua et al. (2021)
C
Patinho et al.
N = 2
DHRS7B
FHL1
Gagaoua et al. (2021)
D
-log10(P)
GO:0050839: cell adhesion molecule binding
GO:0016491: oxidoreductase activity
GO:0009152: purine ribonucleotide biosynthetic process
R-HSA-71291: Metabolism of amino acids and derivatives
GO:0042803: protein homodimerization activity
GO:0006091: generation of precursor metabolites and energy
R-HSA-2262752: Cellular responses to stress
GO:0014823: response to activity
R-HSA-6798695: Neutrophil degranulation
GO:0016835: carbon-oxygen lyase activity
hsa04922: Glucagon signaling pathway
GO:0005080: protein kinase C binding
GO:0051222: positive regulation of protein transport
GO:0042805: actinin binding
hsa00500: Starch and sucrose metabolism
GO:0032787: monocarboxylic acid metabolic process
GO:0033275: actin-myosin filament sliding
R-HSA-8982491: Glycogen metabolism
GO:0009205: purine ribonucleoside triphosphate metabolic process
GO:0006936: muscle contraction
Gagaoua
Patinho
E
-log10(P)
GO:0006941: striated muscle contraction
GO:0042805: actinin binding
hsa01200: Carbon metabolism
GO:0003779: actin binding
GO:0016491: oxidoreductase activity
GO:0032787: monocarboxylic acid metabolic process
GO:0044282: small molecule catabolic process
GO:0042026: protein refolding
GO:0010035: response to inorganic substance
R-HSA-71406: Pyruvate metabolism and Citric Acid (TCA) cycle
GO:0045296: cadherin binding
GO:0006091: generation of precursor metabolites and energy
GO:0003012: muscle system process
R-HSA-114608: Platelet degranulation
GO:0043603: cellular amide metabolic process
R-HSA-2262752: Cellular responses to stress
GO:0016620: oxidoreductase activity, acting on the aldehyde or oxo group of donors, NAD or NADP as accepto
GO:0033275: actin-myosin filament sliding
R-HSA-8982491: Glycogen metabolism
GO:0042803: protein homodimerization activity
Gagaoua
Patinho
F
-log10(P)
GO:0010035: response to inorganic substance
GO:0042180: cellular ketone metabolic process
GO:0044283: small molecule biosynthetic process
GO:0044282: small molecule catabolic process
GO:0006091: generation of precursor metabolites and energy
GO:0003012: muscle system process
GO:0016491: oxidoreductase activity
GO:0042026: protein refolding
GO:0046716: muscle cell cellular homeostasis
GO:0016835: carbon-oxygen lyase activity
GO:0016627: oxidoreductase activity, acting on the CH-CH group of donors
hsa00500: Starch and sucrose metabolism
GO:0005080: protein kinase C binding
hsa04922: Glucagon signaling pathway
GO:0042803: protein homodimerization activity
GO:0051222: positive regulation of protein transport
R-HSA-71387: Metabolism of carbohydrates
R-HSA-8982491: Glycogen metabolism
GO:0033275: actin-myosin filament sliding
GO:0051287: NAD binding
Gagaoua
Patinho

Fig. 8.

Table 1. ANOVA comparison of the meat quality traits evaluated at 72h between normal and high pH groups.

Meat quality traits	Normal pH	High pH	SEM	P-values
pH traits				
pH 24 h	5.72	6.55	0.14	***
pH 44 h	5.71	6.52	0.14	***
pH 72 h	5.58	6.42	0.14	***
Color traits at 72h				
Lightness (*L**)	39.65	34.50	1.26	*
Redness (*a**)	23.88	20.87	0.63	**
Yellowness (*b**)	15.04	12.53	0.58	*
Chroma (*C**)	28.22	24.34	0.84	*
Hue angle (*h*°)	32.11	30.96	0.36	ns
% Methmyoglobin (MetMb, %)	17.24	18.61	0.59	ns
% Deoxymyoglobin (DeoxyMb, %)	22.28	29.08	1.69	*
% Oxymyoglobin (OxyMb, %)	60.48	52.31	1.84	*
Surface color stability	4.69	4.43	0.09	ns
Texture traits at 72h				
Cooking loss, %	24.40	20.83	1.21	ns
Warner-Bratzler Shear force (72h), N	96.08	36.85	11.5	***

Table 2. List of the differentially abundant proteins (DAPs) between high and normal ultimate pH (pHu) beef at 30 min *postmortem* (n = 33).

Uniprot ID	Full protein name	Gene name	Regulation in high pH group	Log2(FC) (high/normal)	Log10(P-value)
Q3Y5Z3	Adiponectin	ADIPOQ	Down	-0.45	1.80
P13214	Annexin A4	ANXA4	Down	-0.41	1.74
Q0VCK0	Bifunctional purine biosynthesis protein PURH	ATIC	Down	-0.35	1.59
P00829	ATP synthase subunit beta, mitochondrial	ATP5B	Down	-0.44	1.51
Q2KJ23	Bridging integrator 1	BIN1	Down	-0.40	1.31
Q27970	Calpain-1 catalytic subunit	CAPN1	Down	-0.44	2.06
Q5EAC6	Hsp90 co-chaperone Cdc37	CDC37	Down	-2.08	2.27
F1MKP6	Cadherin-13	CDH13	Down	-1.54	2.35
F1MPU0	Clathrin heavy chain	CLTC	Down	-0.60	1.54
Q29RK1	Citrate synthase, mitochondrial	CS	Down	-0.63	2.39
Q3MHW9	NADH-cytochrome b5 reductase 1	CYB5R1	Down	-0.98	1.40
P0C591	Dual specificity phosphatase DUPD1	DUPD1	Down	-0.40	1.98
Q3SZ00	HADHA protein	HADHA	Down	-0.45	1.34
O77784	Isocitrate dehydrogenase [NAD] subunit beta, mitochondrial	IDH3B	Down	-0.82	1.74
G3MZU6	Immunoglobulin-like and fibronectin type III domain-containing protein 1	IGFN1	Down	-1.15	2.18
Q3T145	Malate dehydrogenase, cytoplasmic	MDH1	Down	-0.50	2.33
F1N7X3	Nucleosome assembly protein 1-like 4	NAP1L4	Down	-0.84	1.46
P34943	NADH dehydrogenase [ubiquinone] 1 alpha subcomplex subunit 9, mitochondrial	NDUFA9	Down	-0.64	2.17
F1MLD0	4'-phosphopantetheine phosphatase	PANK4	Down	-0.41	1.35
F1MWE0	Homologous-pairing protein 2 homolog	PSMC3	Down	-0.48	1.55
A7MBA2	PSMD1 protein	PSMD1	Down	-0.36	1.78
P12234	Phosphate carrier protein, mitochondrial	SLC25A3	Down	-0.63	1.64
A3KMV5	Ubiquitin-like modifier-activating enzyme 1	UBA1	Down	-0.42	1.91
Q07130	UTP--glucose-1-phosphate uridylyltransferase	UGP2	Down	-0.42	1.35
A5D7J6	CALR protein	CALR	Up	0.68	1.45
Q08E45	Calcium/calmodulin-dependent protein kinase II alpha	CAMK2A	Up	1.68	2.51
Q6EWQ7	Eukaryotic translation initiation factor 5A-1	EIF5A	Up	1.31	1.39

A0A0A0MPA2	Histone H2A	HIST1H2AJ	Up	1.03	1.41
E1B8G9	Histone H2B	HIST3H2BB	Up	1.03	1.71
Q3T003	60S ribosomal protein L18a	RPL18A	Up	1.11	1.53
Q862I1	60S ribosomal protein L24	RPL24	Up	1.15	1.83
Q3T0R1	40S ribosomal protein S18	RPS18	Up	2.07	2.05
A6QLG5	40S ribosomal protein S9	RPS9	Up	1.11	1.75

Table 3. List of the differentially abundant proteins (DAPs) between high and normal ultimate pH (pHu) beef at 9 h *postmortem* (n = 181).

Uniprot ID	Full protein name	Gene name	Regulation in high pH group	Log2(FC) (high/normal)	Log10(P-value)
P44818	Very long-chain specific acyl-CoA dehydrogenase, mitochondrial	ACADVL	Down	-0.38	1.56
P68138	Actin, alpha skeletal muscle	ACTA1	Down	-0.69	1.54
Q3ZC55	Alpha-actinin-2	ACTN2	Down	-0.49	2.52
P07033	Acylphosphatase-2	ACYP2	Down	-0.93	1.36
A7YWE4	Delta-1-pyrroline-5-carboxylate dehydrogenase, mitochondrial	ALDH4A1	Down	-1.27	1.85
F1N7K8	Methylmalonate-semialdehyde dehydrogenase [acylating], mitochondrial	ALDH6A1	Down	-0.74	1.37
F1N5U0	Alpha-protein kinase 3	ALPK3	Down	-2.28	2.69
A2VE25	ANK1 protein	ANK1	Down	-1.80	1.84
F1MD66	Annexin	ANXA11	Down	-0.82	1.64
P13214	Annexin A4	ANXA4	Down	-0.57	1.94
P00829	ATP synthase subunit beta, mitochondrial	ATP5B	Down	-0.29	1.58
P13619	ATP synthase F(0) complex subunit B1, mitochondrial	ATP5F1	Down	-0.93	1.61
P13621	ATP synthase subunit O, mitochondrial	ATP5O	Down	-0.55	2.54
E1BL29	Bleomycin hydrolase	BLMH	Down	-0.91	1.66
G3X7Q7	Voltage-dependent L-type calcium channel subunit beta-1	CACNB1	Down	-0.89	1.49
A6QP82	Calpain 3, (P94)	CAPN3	Down	-1.13	1.42
Q9XSC6	Creatine kinase M-type	CKM	Down	-0.52	1.75
F1MBP8	COP9 signalosome complex subunit 5	COPS5	Down	-1.40	1.62
F1MDK0	COP9 signalosome complex subunit 7a	COPS7A	Down	-1.12	2.01

Q29RI0	Atypical kinase COQ8A, mitochondrial	COQ8A	Down	-0.72	2.32
P00423	Cytochrome c oxidase subunit 4 isoform 1, mitochondrial	COX4I1	Down	-1.03	1.47
P07471	Cytochrome c oxidase subunit 6A2, mitochondrial	COX6A2	Down	-1.55	2.03
F1N7T1	NADH-cytochrome b5 reductase	CYB5R3	Down	-0.82	2.42
P00125	Cytochrome c1, heme protein, mitochondrial	CYC1	Down	-0.78	1.39
E1BDM8	Probable ATP-dependent RNA helicase DDX6	DDX6	Down	-2.54	1.97
F1N206	Dihydrolipoyl dehydrogenase	DLD	Down	-0.70	2.26
A5D989	Elongation factor 1-delta	EEF1D	Down	-0.95	1.55
F1MG05	Elongation factor 1-gamma	EEF1G	Down	-0.88	2.11
P68102	Eukaryotic translation initiation factor 2 subunit 1	EIF2S1	Down	-0.44	2.90
Q3ZC09	Beta-enolase	ENO3	Down	-0.52	1.77
A5PK37	EPM2A protein	EPM2A	Down	-1.59	1.89
Q2KJJ9	Fructose-1,6-bisphosphatase isozyme 2	FBP2	Down	-0.40	1.58
Q3SWX4	Glioblastoma amplified sequence	GBAS	Down	-0.72	2.35
Q5EA88	Glycerol-3-phosphate dehydrogenase [NAD(+)], cytoplasmic	GPD1	Down	-0.53	1.47
P28801	Glutathione S-transferase P	GSTP1	Down	-0.62	1.65
Q3B7M2	Hydroxyacylglutathione hydrolase, mitochondrial	HAGH	Down	-1.26	1.73
P62958	Histidine triad nucleotide-binding protein 1	HINT1	Down	-1.34	2.59
A0A0A0MP90	Histone H2A	HIST1H2AC	Down	-1.18	1.58
E1BMK2	High mobility group protein B1	HMGB1	Down	-0.93	1.75
P19120	Heat shock cognate 71 kDa protein	HSPA8	Down	-0.53	1.33
Q5EAC9	Heat shock protein beta-8	HSPB8	Down	-2.15	1.89
O77784	Isocitrate dehydrogenase [NAD] subunit beta, mitochondrial	IDH3B	Down	-1.23	2.72
A6H7I0	KBTBD5 protein	KBTBD5	Down	-1.17	2.09
F1MD77	Laminin subunit gamma-1	LAMC1	Down	-0.98	1.63
G3N3C9	LIM domain-binding protein 3	LDB3	Down	-0.59	1.64
Q17QE2	LIM and cysteine-rich domains protein 1	LMCD1	Down	-0.53	1.50
F1MYG5	Prelamin-A/C	LMNA	Down	-0.36	1.46
F1N0E2	UPI0000F341DF	LOC520317	Down	-0.71	1.98
Q5E9X2	Dual specificity mitogen-activated protein kinase kinase 6	MAP2K6	Down	-0.88	2.42
P02192	Myoglobin	MB	Down	-0.99	1.92
A4FUD0	MTHFD1 protein	MTHFD1	Down	-1.37	1.85
A6QP89	MYBPC1 protein	MYBPC1	Down	-0.57	1.69

E1BF23	Myomesin-2	MYOM2	Down	-0.51	1.67
F1MPU4	Myotilin	MYOT	Down	-0.39	1.75
Q05752	NADH dehydrogenase [ubiquinone] 1 alpha subcomplex subunit 7	NDUFA7	Down	-1.79	2.75
P42029	NADH dehydrogenase [ubiquinone] 1 alpha subcomplex subunit 8	NDUFA8	Down	-0.85	1.52
Q02367	NADH dehydrogenase [ubiquinone] 1 beta subcomplex subunit 6	NDUFB6	Down	-1.22	1.64
F1MPL4	Nucleoside diphosphate kinase B	NME2	Down	-1.31	2.18
Q3SZC4	NSFL1 cofactor p47	NSFL1C	Down	-1.00	1.95
F1N184	NXPE family member 4	NXPE4	Down	-0.49	1.57
E1BK71	Protein kinase C and casein kinase II substrate protein 3	PACSIN3	Down	-0.59	1.53
F1MJ02	Pre-B-cell leukemia transcription factor 1	PBX1	Down	-0.84	2.87
F1N2K1	Prenylcysteine oxidase 1	PCYOX1	Down	-0.78	1.55
P22439	Pyruvate dehydrogenase protein X component	PDHX	Down	-1.23	1.46
Q3ZBU0	PDZ and LIM domain 5	PDLIM5	Down	-0.54	1.91
Q3SX40	PDZ and LIM domain protein 7	PDLIM7	Down	-0.57	1.47
Q09430	Profilin-2	PFN2	Down	-1.69	1.78
A5PJQ6	PGRMC2 protein	PGRMC2	Down	-1.63	2.97
Q32PA4	14 kDa phosphohistidine phosphatase	PHPT1	Down	-1.88	2.65
A5D984	Pyruvate kinase	PKM2	Down	-0.61	1.60
E1BLN7	Protein phosphatase 1 regulatory subunit 3A	PPP1R3A	Down	-0.68	1.35
P35705	Thioredoxin-dependent peroxide reductase, mitochondrial	PRDX3	Down	-0.62	1.74
F1MQV7	Non-specific serine/threonine protein kinase	PRKAA2	Down	-0.76	1.34
Q1LZE9	Serine protease 23	PRSS23	Down	-0.80	1.57
Q3T0X5	Proteasome subunit alpha type-1	PSMA1	Down	-1.16	1.75
Q32KL2	Proteasome subunit beta type-5	PSMB5	Down	-0.67	1.40
Q2KJ25	26S proteasome non-ATPase regulatory subunit 12	PSMD12	Down	-1.48	2.55
Q3ZBD0	26S proteasome non-ATPase regulatory subunit 7	PSMD7	Down	-0.85	1.78
P61585	Transforming protein RhoA	RHOA	Down	-1.72	1.93
G3MYE2	60S ribosomal protein L5	RPL5	Down	-1.51	2.84
Q3ZBH8	40S ribosomal protein S20	RPS20	Down	-0.89	1.50
F1MZW8	Ribosomal protein S6 kinase	RPS6KA3	Down	-1.23	2.01
Q5E9T9	tRNA-splicing ligase RtcB homolog	RTCB	Down	-1.08	1.93
F6QK60	NAD-dependent protein deacetylase Sirt2	SIRT2	Down	-1.77	1.66
P12234	Phosphate carrier protein, mitochondrial	SLC25A3	Down	-0.83	2.24
E1BPV6	Smoothelin-like protein 1	SMTNL1	Down	-3.35	3.14

F1MNQ4	Superoxide dismutase [Cu-Zn]	SOD1	Down	-0.84	1.88
F1MZ38	Succinate--CoA ligase [ADP/GDP-forming] subunit alpha, mitochondrial	SUCLG1	Down	-0.56	2.42
E1BIS6	Synemin	SYNM	Down	-0.77	1.39
A4IFK4	SYNPO2 protein	SYNPO2	Down	-0.55	1.65
E1B7Z0	TGF-beta-activated kinase 1 and MAP3K7-binding protein 2	TAB2	Down	-1.91	1.41
A0JNC0	Tropomodulin-1	TMOD1	Down	-0.59	1.45
E1BE77	Tripartite motif-containing protein 72	TRIM72	Down	-0.57	1.35
P81947	Tubulin alpha-1B chain	TUBA1B	Down	-0.69	1.37
F1MFL6	Ubiquitin-conjugating enzyme E2 D4	UBE2D4	Down	-0.81	1.60
Q0P5K3	Ubiquitin-conjugating enzyme E2 N	UBE2N	Down	-0.93	2.45
Q3SZ43	Ubiquitin-conjugating enzyme E2 variant 2	UBE2V2	Down	-1.11	1.47
F1MFZ5	Protein unc-45 homolog B	UNC45B	Down	-0.38	1.48
G1K1X0	Cytochrome b-c1 complex subunit 1, mitochondrial	UQCRC1	Down	-0.59	2.22
P23004	Cytochrome b-c1 complex subunit 2, mitochondrial	UQCRC2	Down	-0.36	1.33
F1N789	Vinculin	VCL	Down	-0.52	2.18
A6H783	VDAC5P protein	VDAC5P	Down	-0.55	2.82
F1MTP5	WD repeat-containing protein 1	WDR1	Down	-0.44	1.36
G3MZY7	UPI0002263C8B		Down	0.70	1.46
P12763	Alpha-2-HS-glycoprotein	AHSG	Up	1.89	1.89
P20000	Aldehyde dehydrogenase, mitochondrial	ALDH2	Up	0.89	1.43
F6QVC9	Annexin	ANXA5	Up	1.81	1.41
E1BC10	Amine oxidase	AOC3	Up	2.92	1.32
A5PKI0	APPL1 protein	APPL1	Up	2.33	2.26
F1MY27	BCL2/adenovirus E1B 19 kDa protein-interacting protein 3	BNIP3	Up	0.38	1.67
G3MZ07	Voltage-dependent L-type calcium channel subunit alpha	CACNA1S	Up	3.10	2.11
A5D9F0	Calcium/calmodulin-dependent protein kinase II delta	CAMK2D	Up	1.64	1.45
P13135	Calpain small subunit 1	CAPNS1	Up	1.31	1.38
Q5E997	F-actin-capping protein subunit alpha-2	CAPZA2	Up	0.58	1.39
P79136	F-actin-capping protein subunit beta	CAPZB	Up	1.31	1.50
A4FV37	Caveolae-associated protein 3	CAVIN3	Up	1.63	1.35
F1MAX3	Centrosomal protein of 192 kDa	CEP192	Up	1.40	2.88
E3W9A2	CAP-Gly domain-containing linker protein 1	CLIP1	Up	2.43	1.65
F1ME62	Cardiomyopathy-associated protein 5	CMYA5	Up	3.06	1.80
Q6QTG5	Cytochrome c oxidase subunit 3	COX3	Up	2.51	1.52
O97764	Zeta-crystallin	CRYZ	Up	3.07	1.43
E1BH82	Casein kinase II subunit alpha	CSNK2	Up	3.17	1.97

		A1			
F1N7D7	Dystroglycan	DAG1	Up	4.61	2.08
E1BIK7	Density-regulated protein	DENR	Up	3.03	1.69
Q2HJ94	DnaJ homolog subfamily A member 2	DNAJA2	Up	3.65	1.88
F1N062	Dual specificity phosphatase 27	DUSP27	Up	3.19	1.48
Q56JZ5	Eukaryotic translation initiation factor 3 subunit H	EIF3H	Up	2.64	1.82
Q2KIG0	Electron transfer flavoprotein-ubiquinone oxidoreductase, mitochondrial	ETFDH	Up	1.88	2.03
Q2KJI3	Protein FAM49B	FAM49B	Up	2.66	1.87
F1MR86	Four and a half LIM domains protein 1	FHL1	Up	0.81	1.39
Q3ZBI6	Four and a half LIM domains protein 3	FHL3	Up	2.79	2.26
Q2KJ17	GTPase activating protein (SH3 domain) binding protein 2	G3BP2	Up	4.72	2.19
Q2KJE5	Glyceraldehyde-3-phosphate dehydrogenase, testis-specific	GAPDHS	Up	1.80	1.80
A6QLU1	Glycerol-3-phosphate dehydrogenase, mitochondrial	GPD2	Up	3.54	1.38
F6Q751	Glutathione S-transferase Mu 2	GSTM2	Up	0.53	2.04
F1MMU4	Histone H1x	H1FX	Up	8.41	1.34
F1MK91	Protein-cysteine N-palmitoyltransferase HHAT-like protein	HHATL	Up	1.54	1.46
E1BGN3	Histone H3	HIST2H3D	Up	2.91	1.47
Q3SZV7	Hemopexin	HPX	Up	1.18	1.74
Q0VCX2	78 kDa glucose-regulated protein	HSPA5	Up	0.41	1.61
F1MBR1	Heat shock 27kDa protein 2	HSPB2	Up	0.78	1.91
F1MUZ9	60 kDa heat shock protein, mitochondrial	HSPD1	Up	1.01	1.33
Q58CP0	Isocitrate dehydrogenase [NAD] subunit gamma, mitochondrial	IDH3G	Up	3.42	1.40
G5E5B8	Junctophilin-1	JPH1	Up	2.20	1.81
F1MZL0	Junctional sarcoplasmic reticulum protein 1	JSRP1	Up	3.97	1.49
F1MCF8	Ig-like domain-containing protein	LOC100297192	Up	1.25	1.39
Q2KHU5	O-acetyl-ADP-ribose deacetylase MACROD1	MACROD1	Up	0.69	1.70
F1MAZ1	Microtubule-associated protein	MAP4	Up	1.50	2.12
F6RF62	Myosin light chain 4	MYL4	Up	3.03	2.16
A4IFM7	Myosin light chain kinase 2, skeletal/cardiac muscle	MYLK2	Up	2.43	1.63
Q95KV7	NADH dehydrogenase [ubiquinone] 1 alpha subcomplex subunit 13	NDUFA13	Up	4.31	1.73
Q02369	NADH dehydrogenase [ubiquinone] 1 beta subcomplex subunit 9	NDUFB9	Up	0.45	2.36
Q3ZBH2	NAD(P)H dehydrogenase, quinone 1	NQO1	Up	2.03	1.46
F1MMX	Nebulin-related-anchoring protein	NRAP	Up	5.36	1.75

2					
F1MYV1	NUT family member 1	NUTM1	Up	3.74	1.80
E1B959	Phosphoglycerate mutase	PGAM2	Up	1.70	1.89
F1MJ90	Phosphorylase b kinase regulatory subunit beta	PHKB	Up	1.19	1.86
Q3T0U2	60S ribosomal protein L14	RPL14	Up	2.77	1.35
E1BK63	Ribosomal protein L15	RPL15	Up	1.21	1.77
Q5E973	60S ribosomal protein L18	RPL18	Up	4.30	1.36
G3MYC1	60S ribosomal protein L26	RPL26	Up	4.37	1.38
F1MDN4	60S acidic ribosomal protein P0	RPLP0	Up	1.51	1.33
F1N405	Reticulon	RTN4	Up	3.60	1.46
Q3SWZ6	Ribosome maturation protein SBDS	SBDS	Up	5.61	1.65
G3MY67	Succinate dehydrogenase [ubiquinone] flavoprotein subunit, mitochondrial	SDHA	Up	1.20	1.37
A2I7M9	Serpin A3-2	SERPINA3	Up	3.95	1.83
F1MSZ6	Antithrombin-III	SERPINC1	Up	5.57	1.53
F1MBL6	Serine/threonine-protein kinase SMG1	SMG1	Up	1.08	1.64
F1MZS3	Histone-lysine N-methyltransferase SMYD1	SMYD1	Up	1.35	1.66
F1MDV3	Beta-1-syntrophin	SNTB1	Up	2.48	1.65
F1MQC4	Spermatogenesis-associated protein 22	SPATA22	Up	0.98	1.54
E1BKF8	Signal peptide peptidase-like 2B	SPPL2B	Up	3.52	1.35
E1BA93	Synaptopodin	SYNPO	Up	0.84	1.39
E1BHE1	Serine/threonine-protein kinase TAO3	TAOK3	Up	0.68	1.34
Q3ZCD7	Very-long-chain enoyl-CoA reductase	TECR	Up	0.92	1.85
G3X6N3	Serotransferrin	TF	Up	0.38	1.65
F6Q3H3	TELO2-interacting protein 1 homolog	TTI1	Up	1.90	1.85
Q3MHP1	Ubiquitin-conjugating enzyme E2 L3	UBE2L3	Up	1.37	1.87
E1BEW9	WD repeat-containing protein 87	WDR87	Up	4.89	2.16
A0A140T894	14-3-3 protein beta/alpha	YWHAB	Up	4.25	1.40
G3MXM1	UPI00006157C1		Up	-0.86	1.60

Table 4. List of the differentially abundant proteins (DAPs) between high and normal ultimate pH (pHu) beef at 44 h *postmortem* (n = 37).

Uniprot ID	Full protein name	Gene name	Regulation in high pH group	Log2(FC) (high/normal)	Log10(P-value)
A2VE25	ANK1 protein	ANK1	Down	-1.73	1.35
F1MIU2	BAG family molecular chaperone regulator 3	BAG3	Down	-1.69	1.73
F1N7T1	NADH-cytochrome b5 reductase	CYB5R3	Down	-0.70	1.37
F1MN23	Dehydrogenase/reductase SDR family member 7B	DHRS7B	Down	-0.41	1.33
P00125	Cytochrome c1, heme protein, mitochondrial	CYC1	Down	-0.31	1.36
Q1RMM6	Coenzyme Q10 homolog A	COQ10A	Down	-0.60	1.67
P01966	Hemoglobin subunit alpha	HBA	Down	-0.70	1.59
A6QLD3	LRRC20 protein	LRRC20	Down	-0.78	1.82
Q3SZH7	Leukotriene A-4 hydrolase	LTA4H	Down	-0.98	1.37
P02192	Myoglobin	MB	Down	-0.44	1.74
Q05752	NADH dehydrogenase [ubiquinone] 1 alpha subcomplex subunit 7	NDUFA7	Down	-0.69	1.41
P34943	NADH dehydrogenase [ubiquinone] 1 alpha subcomplex subunit 9, mitochondrial	NDUFA9	Down	-0.29	1.37
Q5E946	Protein DJ-1	PARK7	Down	-0.88	1.38
F1MNQ4	Superoxide dismutase [Cu-Zn]	SOD1	Down	-0.87	1.36
P41976	Superoxide dismutase [Mn], mitochondrial	SOD2	Down	-0.35	1.35
A0JNC0	Tropomodulin-1	TMOD1	Down	-0.31	1.32
P81947	Tubulin alpha-1B chain	TUBA1B	Down	-0.87	1.40
F1MFZ5	Protein unc-45 homolog B	UNC45B	Down	-0.77	1.58
Q0II26	Aminoacyl tRNA synthase complex-interacting multifunctional protein 2	AIMP2	Up	2.01	1.45
P20000	Aldehyde dehydrogenase, mitochondrial	ALDH2	Up	0.76	1.45
A2VDL6	Sodium/potassium-transporting ATPase subunit alpha-2	ATP1A2	Up	0.63	1.41
A5PJI6	Caveolae-associated protein 4	CAVIN4	Up	1.10	1.32
Q2HJ94	DnaJ homolog subfamily A member 2	DNAJA2	Up	2.23	1.36
Q3T0U3	Es1 protein	ES1	Up	1.20	1.63
F1MR86	Four and a half LIM domains protein 1	FHL1	Up	0.55	1.35
Q2KJ	Glyceraldehyde-3-phosphate dehydrogenase,	GAPD	Up	0.91	1.35

E5	testis-specific	HS			
F1MP10	COP9 signalosome complex subunit 1	GPS1	Up	1.31	2.24
F6Q751	Glutathione S-transferase Mu 2	GSTM2	Up	0.60	1.77
Q0IIJ2	Histone H1.0	H1F0	Up	2.14	1.31
Q2HJD7	3-hydroxyisobutyrate dehydrogenase, mitochondrial	HIBADH	Up	2.19	1.51
Q2KHU9	Heat shock protein beta-3	HSPB3	Up	0.84	1.42
Q58CP0	Isocitrate dehydrogenase [NAD] subunit gamma, mitochondrial	IDH3G	Up	1.69	1.37
F1MVX2	Glutathione S-transferase LANCL1	LANCL1	Up	0.40	2.10
A2I7M9	Serpin A3-2	SERPINA3	Up	2.01	1.58
F1MSZ6	Antithrombin-III	SERPINC1	Up	2.63	1.33
Q0P5E6	Alpha-1-syntrophin	SNTA1	Up	0.56	1.49
Q3MHP1	Ubiquitin-conjugating enzyme E2 L3	UBE2L3	Up	1.06	1.41

Declaration of Competing Interest

No potential conflict of interest was reported by the authors.

CRediT authorship contribution statement

Iliani Patinho: Conceptualization, Data curation, Formal Analysis, Investigation, Methodology, Visualization, Writing – original draft. **Daniel S. Antonelo:** Formal Analysis, Software, Visualization, Writing – review & editing. **Eduardo F. Delgado:** Writing – review & editing. **Laura Alessandroni:** Data curation, Formal Analysis, Visualization, Writing – review & editing. **Julio C.C. Balieiro:** Supervision, Writing – review & editing. **Carmen J. Contreras-Castillo:** Conceptualization, Funding acquisition, Supervision, Writing – review & editing. **Mohammed Gagaoua:** Conceptualization, Data curation, Formal Analysis, Funding acquisition, Investigation, Methodology, Project administration, Resources, Software, Supervision, Validation, Visualization, Writing – original draft, Writing – review & editing

Highlights

- In-depth proteomics exploration of dark-cutting beef condition using three muscle sampling times taken early *postmortem*
- 251 proteins were differentially expressed creating the most comprehensive interconnected pathways of high-pHu beef
- Energy metabolism, cellular stress response and oxidoreductase activity play pivotal roles
- Ribosomal proteins and histones play pivotal role in dark-cutting beef development
- Pathways are proposed to determine the biological mechanisms behind dark-cutting beef